ARTICLE

SIRT1–NOX4 signaling axis regulates cancer cachexia

Aneesha Dasgupta[1], Surendra K. Shukla[2], Enza Vernucci[2], Ryan J. King[2], Jaime Abrego[2], Scott E. Mulder[1], Nicholas J. Mullen[2], Gavin Graves[2], Kyla Buettner[2], Ravi Thakur[2], Divya Murthy[2], Kuldeep S. Attri[2], Dezhen Wang[2], Nina V. Chaika[2], Camila G. Pacheco[2], Ibha Rai[2], Dannielle D. Engle[3], Paul M. Grandgenett[2], Michael Punsoni[4], Bradley N. Reames[5], Melissa Teoh-Fitzgerald[1], Rebecca Oberley-Deegan[1], Fang Yu[6], Kelsey A. Klute[7], Michael A. Hollingsworth[2], Matthew C. Zimmerman[8], Kamiya Mehla[2], Junichi Sadoshima[9], David A. Tuveson[3], and Pankaj K. Singh[1,2,4]

Approximately one third of cancer patients die due to complexities related to cachexia. However, the mechanisms of cachexia and the potential therapeutic interventions remain poorly studied. We observed a significant positive correlation between SIRT1 expression and muscle fiber cross-se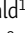ctional area in pancreatic cancer patients. Rescuing _Sirt1_ expression by exogenous expression or pharmacological agents reverted cancer cell–induced myotube wasting in culture conditions and mouse models. RNA-seq and follow-up analyses showed cancer cell–mediated SIRT1 loss induced NF-κB signaling in cachectic muscles that enhanced the expression of FOXO transcription factors and NADPH oxidase 4 (_Nox4_), a key regulator of reactive oxygen species production. Additionally, we observed a negative correlation between NOX4 expression and skeletal muscle fiber cross-sectional area in pancreatic cancer patients. Knocking out _Nox4_ in skeletal muscles or pharmacological blockade of Nox4 activity abrogated tumor-induced cachexia in mice. Thus, we conclude that targeting the Sirt1–Nox4 axis in muscles is an effective therapeutic intervention for mitigating pancreatic cancer–induced cachexia.

Introduction

Cancer cachexia is a metabolic syndrome that contributes to significant mortality in cancer patients (Baracos et al., 2018). It is defined as the loss in skeletal muscle mass that cannot be fully reversed by conventional nutritional therapy and leads to progressive functional impairment (Fearon et al., 2011). While the incidence varies across different cancers, pancreatic ductal adenocarcinoma (PDAC) patients show the highest prevalence of cancer cachexia (Baracos et al., 2018). According to an estimate, one third of pancreatic cancer patients die directly due to cachexia-associated complications, entailing respiratory or cardiac failure (Bachmann et al., 2009). Cancer cachexia is also associated with poor response to chemotherapy and decreased overall survival (Bachmann et al., 2008; Dewys et al., 1980). Until now, the manifestation of cancer cachexia has been attributed to systemic inflammation caused by the host body and tumor-derived cytokines (Ebrahimi et al., 2004; Fearon et al., 2006). However, there are no Food and Drug Administration–approved drugs to mitigate cancer-induced cachexia. Thus, there is an urgent need to find more effective therapeutic targets against cancer cachexia.

The silent information regulator 2 (SIR2) family of proteins, called sirtuins, are primarily NAD$^+$-dependent protein deacylases and mono-[ADP-ribosyl] transferases that link changes in energy metabolism to transcriptional reprogramming (Imai et al., 2000). These enzymes respond to the availability of NAD$^+$ which is an important currency in energy homeostasis and cellular metabolism (Imai and Guarente, 2016). There are seven mammalian sirtuins, which are also referred to as class III histone deacetylases (Bosch-Presegué and Vaquero, 2011). Sirtuins vary in their subcellular localization and their preferred substrates, which in turn define their specific roles in cellular homeostasis (German and Haigis, 2015). Mammalian sirtuins are involved in various functions such as chromatin regulation, metabolic homeostasis, and cell survival under stress (Bosch-Presegué and Vaquero, 2011). Introducing an additional copy of _sir-2_ gene enhances the lifespan of _Caenorhabditis elegans_ by 50%, and its inhibition leads to a shortened lifespan (Tissenbaum and Guarente, 2001), implying an essential role of sirtuins in aging.

....
[1]Department of Biochemistry and Molecular Biology, University of Nebraska Medical Center, Omaha, NE;   [2]The Eppley Institute for Research in Cancer and Allied Diseases, University of Nebraska Medical Center, Omaha, NE;   [3]Cancer Center at Cold Spring Harbor Laboratory, Cold Spring Harbor, NY;   [4]Department of Pathology and Microbiology, University of Nebraska Medical Center, Omaha, NE;   [5]Department of Surgery, University of Nebraska Medical Center, Omaha, NE;   [6]Department of Biostatistics, University of Nebraska Medical Center, Omaha, NE;   [7]Department of Internal Medicine, University of Nebraska Medical Center, Omaha, NE;   [8]Department of Cellular and Integrative Physiology, University of Nebraska Medical Center, Omaha, NE;   [9]Department of Cell Biology and Molecular Medicine, New Jersey Medical School, Rutgers University, Newark, NJ.

Correspondence to Pankaj K. Singh: pankaj.singh@unmc.edu;   D.D. Engle's present address is Salk Institute for Biological Studies, La Jolla, CA.

Among all the sirtuins, Sirt1 has also been illustrated to play a role in muscle physiology (Pardo and Boriek, 2011; Sharples et al., 2015; Vinciguerra et al., 2010) by enhancing mitochondrial fatty acid oxidation through deacetylating peroxisome proliferator-activated receptor-gamma coactivator 1-α (PGC1-α; Amat et al., 2009). Sirtuins also plays a critical role in balancing muscle cell differentiation and proliferation (Fulco et al., 2008; Fulco et al., 2003; Rathbone et al., 2009). It is now well established that increased expression of muscle-specific ubiquitin ligases muscle ring finger 1 (MuRF1) and muscle atrophy F-box (MAFbx/Atrogin-1) is a hallmark of muscle atrophy (Bodine et al., 2001; Gomes et al., 2001). These genes are activated by the FOXO (Forkhead box O) family of transcription factors, including FOXO1 and FOXO3 (Mammucari et al., 2007; Zhao et al., 2007). Activities of FOXO1 and FOXO3 are regulated by cycles of acetylation and deacetylation, the latter being mediated by Sirt1 (Yang et al., 2005). Additionally, decreased SIRT1 in muscle following prolonged fasting correlated with an increase in the levels of ubiquitin ligases (Lee and Goldberg, 2013). Intriguingly, our current study demonstrated a tumor-induced decrease in Sirt1 in the muscles of cancer patients and spontaneous PDAC mouse models.

In this study, we elucidated the potential utility of targeting sirtuins in combating cancer cachexia. We investigated whether activation of sirtuins in the muscle, irrespective of the effects in the tumor, would be sufficient to combat muscle wasting. Moreover, there is growing evidence of oxidative damage in cancer-induced cachexia, and studies have demonstrated successful mitigation of cancer-induced muscle atrophy by the use of antioxidants (Ábrigo et al., 2018; Buck and Chojkier, 1996; Gomes-Marcondes and Tisdale, 2002). Since SIRT1 has been shown to inhibit oxidative stress (Salminen et al., 2013; Zhang et al., 2017), we evaluated its potential to combat oxidative stress-related atrophy in cancer-induced cachexia. Our findings demonstrate that SIRT1 stabilization in the skeletal muscles can mitigate cancer-induced muscle wasting. We have also established a novel function of SIRT1 in the regulation of NADPH oxidase 4 (Nox4) in the muscle tissues of tumor-bearing mice. Furthermore, pharmacological inhibition or genetic deletion of Nox4 enzyme abrogated cancer-induced muscle wasting in tumor-bearing mice and provided a survival benefit.

Results

SIRT1 expression decreases in cancer-induced cachexia
To evaluate whether sirtuins are altered in cachexia, we measured the mRNA expression levels of the seven sirtuins in the gastrocnemius muscles from 10-, 15-, and 25-wk-old $Kras^{LSL.G12D/+}$; $p53^{LSL.R172H/+}$; $Pdx1$-Cre (KPC) spontaneous PDAC tumor-bearing mouse model and littermate controls. $Sirt1$ expression was significantly decreased in gastrocnemius muscles from KPC mice at 15 and 25 wk of age compared with control mice (Fig. 1 A). However, we observed no significant alterations in the other sirtuins, except for $Sirt2$, which was decreased in the KPC mice muscles only at 25 wk of age (Fig. S1 A). Loss in muscle weight was observed in the mice at 15 and 25 wk of age which corresponded to decreased $Sirt1$ expression and increased tumor

progression (Fig. S1, B and C). We also observed an increase in atrophy markers in the muscles of the mice at 15 and 25 wk of age (Fig. S1 D). Concordantly, muscles collected from C26 tumor-bearing mice also demonstrated a decrease in $Sirt1$ expression, with no significant decrease in the other sirtuins (Fig. S1 E).

We next assessed if PDAC patients had a similar decrease in SIRT1 expression in skeletal muscles. To achieve this, we performed immunohistochemical analysis for SIRT1 expression on 54 pancreatic cancer patient skeletal muscle sections obtained from the Rapid Autopsy Program at the University of Nebraska Medical Center (UNMC; Fig. 1 B). We scored the patient muscle samples for SIRT1 staining and observed a significant positive correlation between muscle cross-section area and SIRT1 staining after adjusting the P value for confounding factors (Fig. 1 C and Table S1).

Cancer cell–secreted factors diminish $Sirt1$ expression in C2C12 myotubes
Reasoning that the muscle cells of PDAC patients and tumor-bearing mice respond to factors in the bloodstream, we sought to determine if cancer cell–secreted factors could directly diminish Sirt1 expression in an in vitro C2C12 myotube model. To achieve this, we treated C2C12 myotubes with conditioned media (CM) from human (S2-013 and T3M4) and mouse (KPC1245 and KPC1199) pancreatic cancer cell lines. We observed that $Sirt1$ mRNA levels decreased in C2C12 myotubes upon treatment with PDAC cell line CM (Fig. 1 D). No other sirtuin showed consistently altered expression in this system (Fig. S2 A). Decreased $Sirt1$ expression also correlated with decreased SIRT1 activity, as measured with fluorescence-based activity assays (Fig. 1 D and Fig. S2 B). To exclude the possibility that nutrient deprivation might be driving myotube atrophy in vitro, we performed metabolomics analysis on DMEM, PDAC cell CM, and pancreatic epithelial cell (HPNE)–CM to evaluate the nutrient levels (Fig. S2 C). We then supplemented S2-013 CM with all nutrients that were decreased at least 25% compared with DMEM to bring their levels back up to those in control conditions. We observed no rescue in the cachectic phenotype with the supplemented CM, implying that nutrient starvation is not responsible for myotube thinning (Fig. S2, D and E). Thus, nutrient depletion is not the cause of CM-induced cachexia in our in vitro model.

Exogenous expression or stabilization of SIRT1 expression impedes myotube degeneration and cachexia
To test if Sirt1 stabilization rescues the cachectic phenotype, we overexpressed $Sirt1$ by adenoviral transduction in C2C12-derived myotubes and then treated them with cancer cell CM for 24 h. Sirt1 overexpression ameliorated the cachectic phenotype by every metric that was tested, including myotube thickness (Fig. 1, E and F), total protein content (Fig. 1 G), myosin heavy chain expression (Fig. 1 H), and mRNA expression of $Trim63$ and $Fbxo32$ muscle-specific ubiquitin ligases (Fig. 1, I and J). These changes were not caused by myotube apoptosis, as caspase 3/7 activity assays showed no increase upon CM treatment (Fig. S2 E).

Next, we evaluated if enhancing SIRT1 levels with a pharmacologically relevant compound would prevent skeletal muscle
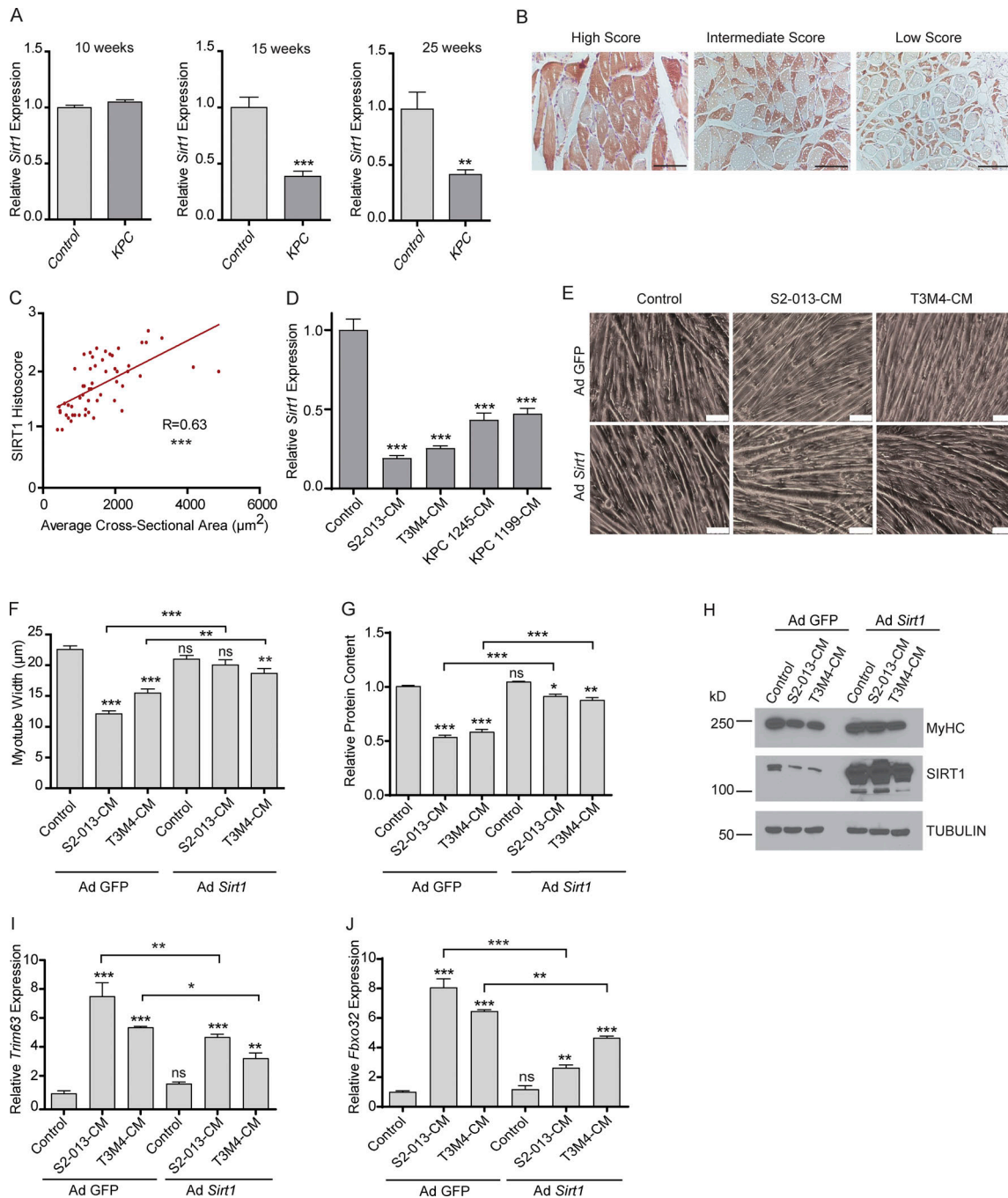
Figure 1. **Sirt1 expression decreases in cachectic muscles. (A)** *Sirt1* mRNA expression in KPC mouse gastrocnemius muscles (*n* = 3) at 10, 15, and 25 wk after birth. **(B)** Representative immunohistochemical micrographs of SIRT1 staining in skeletal muscles of pancreatic cancer patients. **(C)** Correlation of the average skeletal muscle fiber cross section area with the SIRT1 histoscore in 54 muscle autopsy samples of pancreatic cancer patients. R depicts Pearson's correlation coefficient and P < 0.0001. **(D)** *Sirt1* mRNA expression in myotubes treated with S2-013, T3M4, KPC1245, and KPC1199 CM for 24 h. **(E–J)** Brightfield microscopy images (at 200×; E), myotube width quantification (F), relative protein content (G), protein lysate immunoblot analysis of MyHC (H), and mRNA expression of *Trim63* (MuRF-1) and *Fbxo32* (Atrogin-1; I and J) in C2C12 myotubes transfected with either adenoviral GFP or Sirt1 and treated with S2-013 and T3M4-CM for 24 h. Scale bars represent 75 µm. Data are presented as mean ± SEM and were compared with Student's *t* test (A), one-way ANOVA with Dunnett's (D), or Bonferroni's (F, G, I, and J) multiple comparisons. *, P < 0.05; **, P < 0.01; ***, P < 0.001. ns, not significant. All the in vitro experiments were verified in at least two independent experiments.

wasting. Previous studies have established that resveratrol (3,5,4′-trihydroxystilbene), a natural phytoalexin, increases the deacetylase activity of SIRT1 (Howitz et al., 2003) and increases SIRT1 expression (Dong et al., 2014; Lagouge et al., 2006; Wu et al., 2015). Since we observed that *Sirt1* levels were decreased in cachectic muscles, we investigated if resveratrol could revert the cachectic phenotype. Supplementing the cancer cell CM with resveratrol (50 µM) rescued C2C12 myotube degeneration in

culture conditions, as measured by myotube thickness (Fig. 2, A and B) and myosin heavy chain expression (Fig. 2 C). Resveratrol also diminished the cancer cell CM–induced protein expression of ATROGIN-1 and MuRF1 muscle-specific ubiquitin ligases (Fig. 2 C). The mRNA levels of MuRF1 (*Trim63*) and Atrogin-1 (*Fbxo32*) were also decreased upon addition of resveratrol to the CM (Fig. 2, D and E). We also observed resveratrol-mediated rescue of *Sirt1* mRNA levels in the myotubes upon treatment with CM (Fig. 2 F).

Systemic administration of pharmacological agents stabilizing/increasing Sirt1 expression could diminish cachexia by directly impacting Sirt1 levels in skeletal muscles or by modulating Sirt1 levels in tumor cells that may impact the cachectic secretome of the latter. Hence, it was important to first evaluate the effect of resveratrol on pancreatic cancer cell lines. Of note, previous studies have demonstrated that resveratrol decreases proliferation of some pancreatic cancer cells (Xu et al., 2015; Yang et al., 2014; Zhou et al., 2011). To determine if treatment of pancreatic cancer cell lines with resveratrol impacted cell proliferation in our cell line models, we treated S2-013 and T3M4 cells with multiple doses of resveratrol. We observed that treatment with resveratrol decreased cell proliferation in a dose-dependent manner (Fig. 2 G). The decreased cell proliferation by resveratrol was Sirt1 dependent, because Ex-527, a SIRT1 inhibitor (Oon et al., 2015), could rescue the decreased survival (Fig. S3 A). To further test if SIRT1 contributed to the diminished survival by resveratrol and develop a model to test the effect of resveratrol on the muscle, independent of its effect on the tumor, we generated *SIRT1* knockdowns in S2-013 cells by lentiviral delivery of short hairpin RNAs against *SIRT1*. We used two constructs targeting independent regions of *SIRT1* (sh*SIRT1*-A and sh*SIRT1*-B) for knocking down *SIRT1* expression (Fig. 2 H). We then investigated if *SIRT1* knockdown altered the sensitivity of cancer cells to resveratrol (25 µM) by performing MTT (3-(4,5-dimethylthiazol-2-yl)-2,5-diphenyltetrazolium bromide) assays. We observed that *SIRT1* knockdown cells lacked sensitivity to resveratrol (Fig. 2 I). Cancer cell CM from the scrambled control and the *SIRT1* knockdown cell lines had similar effect on the protein content of the myotubes, implying that modulation of *SIRT1* in the tumor has no impact on the myodegenerative potential in vitro (Fig. 2 J).

Having established that S2-013 cell lines with stable SIRT1 knockdown are resistant to resveratrol, we next investigated if increasing the expression of Sirt1 in skeletal muscles by resveratrol would rescue cachexia in animal models, independent of tumor burden. We implanted scrambled control and *SIRT1* knockdown S2-013 cells orthotopically into the pancreas of athymic nude mice and administered resveratrol (200 mg/kg) daily by oral gavage, starting 6 d after implantation (Fig. 3 A). Consistent with our in vitro results, we observed decreased tumor weight and volume upon necropsy in resveratrol-treated mice implanted with scrambled control cells, but not in those implanted with *SIRT1* knockdown cells (Fig. 3, B and C). We noted decreased body weight and muscle weight in mice implanted orthotopically with tumor cells (Fig. 3, D and E), but not in PBS-injected mice (Fig. S3 B). These results establish the utility of mice implanted with SIRT1 knockdown S2-013 cells for testing the muscle-intrinsic effects of resveratrol.

Using the control and *SIRT1* knockdown S2-013 orthotopic tumor models, we observed that resveratrol ameliorated the PDAC cell–induced cachexia by all metrics tested, including body weight (Fig. 3 D); gastrocnemius muscle weight and cross-sectional area (Fig. 3, E and F); forelimb grip strength (Fig. 3 G); body fat percentage (Fig. 3 H); muscle expression of myosin heavy chain, ATROGIN-1, and MuRF1 (Fig. 3 I); and adipose tissue expression of fat-wasting markers, including *Zag* and *Ucp2*, but not *Ucp1* and *Ucp3* (Fig. S3 C). This profound phenotypic reversal correlated with muscle Sirt1 stabilization as measured by immunoblot and immunohistochemical staining (Fig. 3 I) and Fig. S3 D). Importantly, none of these parameters were significantly influenced by the SIRT1 status of the implanted S2-013 cells or tumor burden at necropsy, suggesting a tumor cell–independent mechanism for resveratrol-mediated reversal of cachexia in tumor-bearing mice.

SIRT1 regulates NF-κB and FOXO transcription factors

To investigate the potential mechanism of action of resveratrol-induced protection against muscle wasting, we performed RNA sequencing (RNA-seq) analysis of myotubes treated with S2-013-CM with or without resveratrol for 24 h. We performed gene set enrichment analysis (GSEA) and determined the enrichment for transcription factors in the transcription factor gene set from TFactS (http://www.tfacts.org/) to evaluate the significantly altered pathways in all the cohorts (Fig. 4 A). We observed significant alterations in 9 out of 101 transcription factor pathways (Fig. 4 B). Of note, we observed enrichment of FOXO1 and FOXO3 transcription factor–regulated genes, which include muscle-specific ubiquitin ligases (Reed et al., 2012; Sandri et al., 2004; Fig. 4 C), and these enrichments were abolished by resveratrol treatment. Additionally, the NF-κB pathway, which has been shown to be a major player in the development of cachexia (Han et al., 1999), was significantly up-regulated, and this enrichment too was abrogated by resveratrol treatment (Fig. 4 D). These results are in line with previous publications demonstrating the regulation of NF-κB activity by Sirt1-mediated deacetylation (Chen et al., 2016; Jang et al., 1997; Kauppinen et al., 2013).

We validated the RNA-seq results by evaluating the mRNA and protein levels of *Foxo1* and *Foxo3* in myotubes treated with cancer cell CM with or without resveratrol. We observed that resveratrol decreased the cancer cell CM–induced expression of the genes encoding for FOXO transcription factors (Fig. 4 E). Similar results were observed in the protein levels of FOXO1 and FOXO3 (Fig. 4 F), confirming that resveratrol prevents muscle wasting by modulating FoxO proteins. We also observed a decrease in the mRNA levels of the *Foxo1* and *Foxo3* upon *Sirt1* overexpression in CM-treated myotubes (Fig. 4 G). These results indicate that *Sirt1* overexpression was sufficient to abrogate the CM-induced expression of FOXO proteins.

A promoter-reporter assay with an NF-κB–responsive promoter-luciferase reporter construct also showed that resveratrol diminished the cancer cell CM–induced NF-κB transcriptional activity in myotubes (Fig. 4 H). Previous studies have demonstrated increased transcriptional activity of NF-κB upon acetylation of p65 at lysine 310 (Chen et al., 2002). Since K310
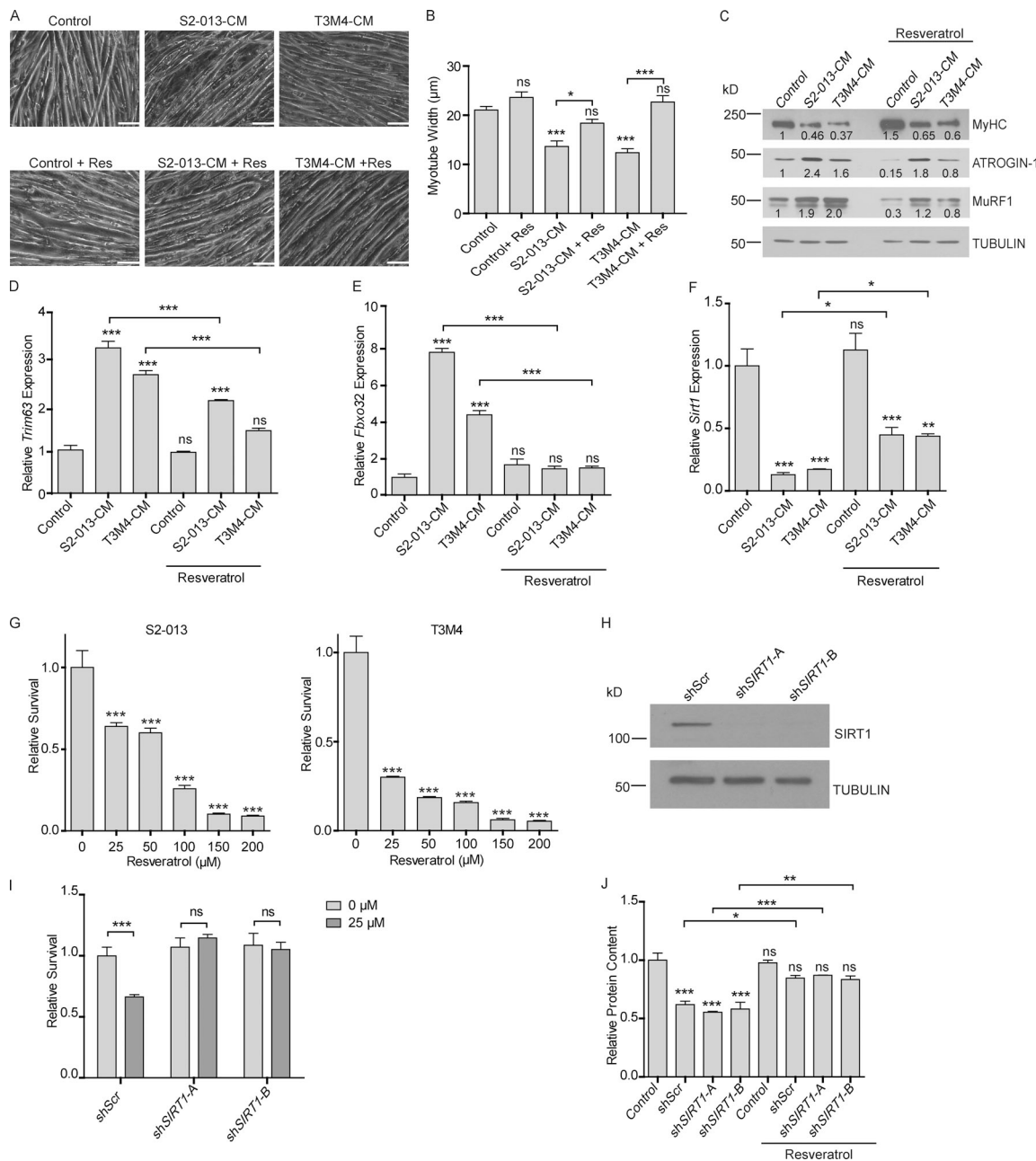
Figure 2. **Modulation of SIRT1 levels by resveratrol combats muscle wasting in vitro. (A)** Brightfield microscopy images (at 200×) of myotubes treated with S2-013 and T3M4 CM with and without resveratrol (50 μM) treatment for 24 h. Scale bars represent 50 μm. **(B)** Myotube width was measured by ImageJ. Five measurements were taken along the length of each myotube. **(C)** Immunoblots of MyHC, Atrogin-1, and MuRF-1 in myotubes treated with S2-013 and T3M4 CM along with resveratrol treatment for 24 h. Tubulin was used as a loading control. Quantification of band intensity was performed via Li-Cor Image Studio Lite and values normalized to the untreated control and to tubulin are indicated below the bands. **(D–F)** mRNA expression of *Trim63* (MuRF-1), *Fbxo32* (Atrogin-1), and *Sirt1* in myotubes treated with S2-013 and T3M4 CM along with resveratrol (50 μM) for 24 h. **(G)** MTT assay demonstrating the dose-dependent effect of resveratrol on S2-013 and T3M4 cell survival 72 h after treatment. **(H)** Immunoblot of SIRT1 in S2-013 cells. Tubulin was used as a loading control. **(I)** Relative survival of S2-013 shScr, shSIRT1-A, and shSIRT1-B upon resveratrol treatment for 72 h (25 μM) by MTT assays. **(J)** Protein content in myotubes treated with S2-013 shScr CM, S2-013 shSIRT1-A CM, S2-013 shSIRT1-B CM along with resveratrol (50 μM). All the experiments were performed at least three times in triplicate. Data are mean ± SEM compared with one-way ANOVA with Bonferroni's (B, D–F, and J) or Dunnett's (G) multiple comparisons. A two-way ANOVA with Bonferroni's post-hoc analysis was used considering the interaction between treatment and cell line (I). *, P < 0.05; **, P < 0.01; ***, P < 0.001. All the in vitro experiments were verified in at least two independent experiments.

residue of p65 has been known to be deacetylated by SIRT1 (Ghisays et al., 2015), we evaluated K310 acetylation levels upon treatment of myotubes with cancer cell CM with and without resveratrol. We observed increased acetylation of p65 at lysine 310 upon cancer cell CM treatment, and the effect was abolished by resveratrol treatment (Fig. 4 I). These data suggest that SIRT1-mediated deacetylation of NF-κB counteracts cancer cell CM–induced NF-κB transcriptional activity in myotubes.
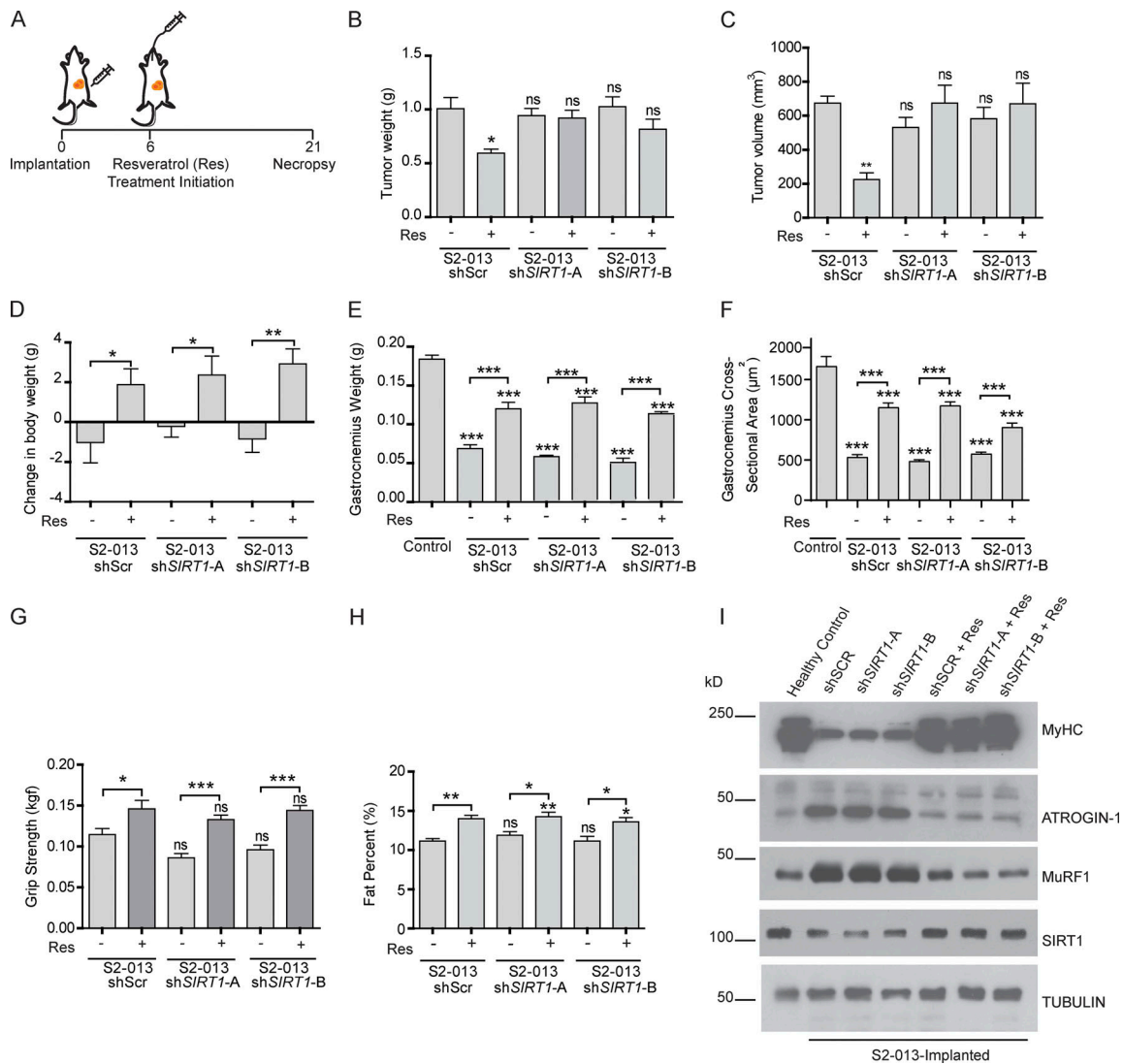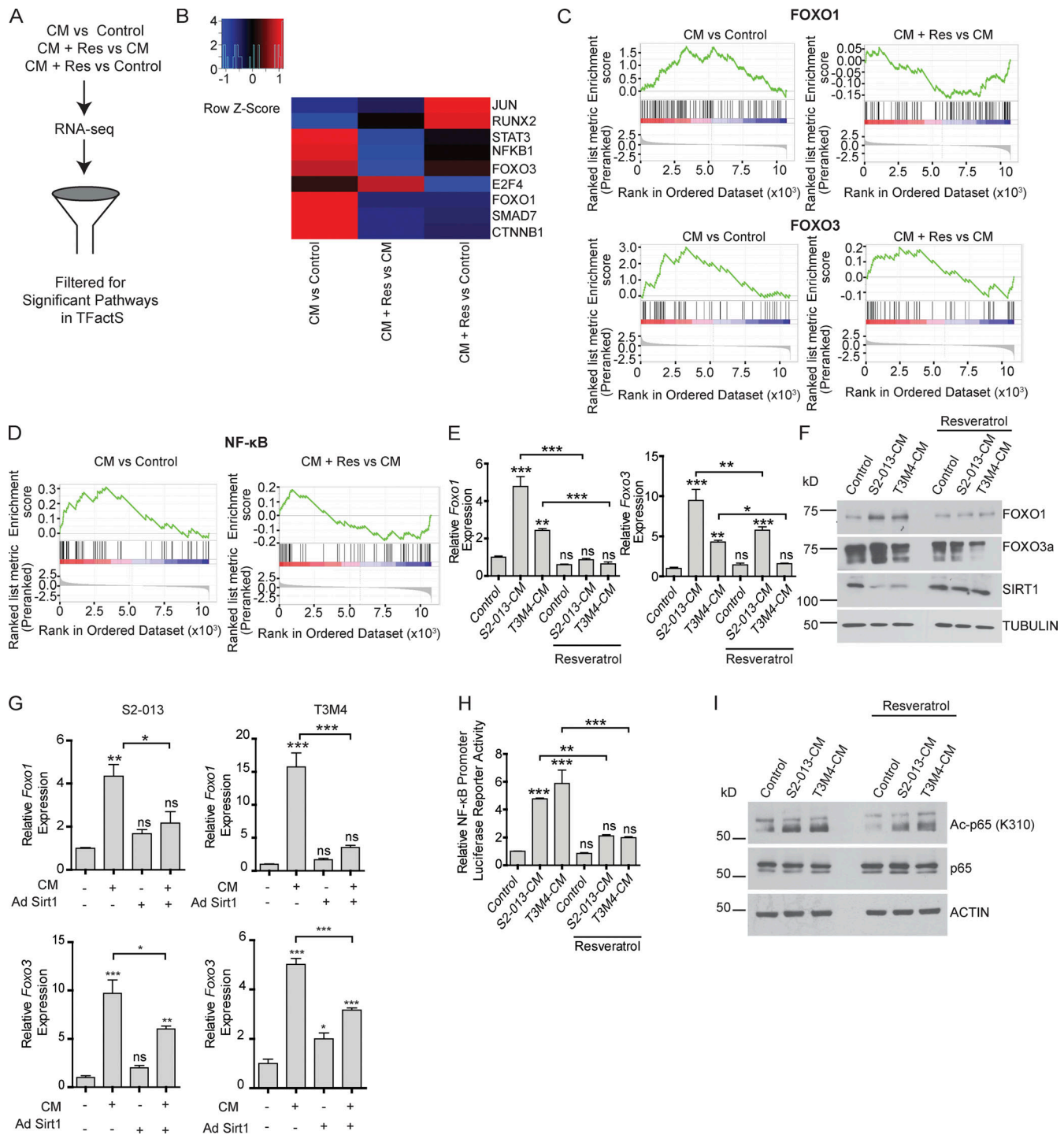
Figure 3. **SIRT1 stabilization in muscles regulates muscles wasting in vivo. (A)** Schematic illustration of the treatment strategy. **(B and C)** Postnecropsy measurements of S2-013 shScr (*n* = 10), sh*SIRT1*-A (*n* = 10), and sh*SIRT1*-B (*n* = 10) tumor weights (B) and tumor volumes (C). **(D)** Change in body weight measurements of the tumor-bearing mice 21 d after implantation. **(E)** Postnecropsy gastrocnemius muscle weight from S2-013 shScr, S2-013 sh*SIRT1*-A, and S2-013 sh*SIRT1*-B tumor-bearing mice. **(F)** Quantification of muscle fiber cross-sectional area in hematoxylin and eosin–stained muscle sections from tumor-bearing mice. **(G)** Measurement of grip strength of the tumor-bearing mice 18 d after implantation. **(H)** Measurement of fat percentage of S2-013 shScr (*n* = 8), S2-013 sh*SIRT1*-A (*n* = 8), and S2-013 sh*SIRT1*-B (*n* = 8) tumor-bearing mice by dual-energy x-ray absorptiometry scanning 18 d after implantation. **(I)** Immunoblots of muscle tissue extracts from the tumor-bearing mice treated with resveratrol or solvent control, showing regulation of MyHC, Atrogin-1, MuRF1, and SIRT1. Tubulin was used as a loading control. All in vitro experiments were performed at least three times in triplicate. Data are mean ± SEM compared with one-way ANOVA with Bonferroni's multiple comparisons (B–H); *, $P < 0.05$; **, $P < 0.01$; ***, $P < 0.001$.

## Diminished SIRT1 expression facilitates Nox4 expression via the induction of NF-κB

Oxidative stress plays very important role in muscle homeostasis (Musarò et al., 2010), and previous studies have established an inverse relationship between SIRT1 and ROS levels in neuronal cells (Khan et al., 2012). Hence, we investigated if diminished SIRT1 levels in cachectic muscles contributed to oxidative damage, resulting in myodegeneration. We observed increased ROS levels in the myotubes treated with cancer cell CM, which was abolished by resveratrol treatment (Fig. 5 A). Thus, we next evaluated the levels of the key enzymes responsible for ROS homeostasis in the muscles of the tumor-bearing

mice treated with resveratrol (Fig. 5 B and Fig. S3 E). We observed increased mRNA and protein expression levels of NADPH oxidase 4 (*Nox4*) that were reversed by resveratrol treatment (Fig. 5 B and Fig. S4 A). This is consistent with previous reports showing regulation of Nox4 by NF-κB in different contexts (Manea et al., 2010; Williams et al., 2012).

Overexpression of *Sirt1* in C2C12 myotubes was sufficient to decrease acetylation of p65 and diminish the induction of Nox4 expression (Fig. S4 B), suggesting a direct role of SIRT1 in NOX4 regulation. To determine if *Nox4* is directly regulated by NF-κB in cachectic skeletal muscles, we performed chromatin immunoprecipitation (ChIP) for NF-κB (p65 subunit) in

Dasgupta et al.
Targeting Sirt1–Nox4 signaling in cancer cachexia

Journal of Experimental Medicine   6 of 17
https://doi.org/10.1084/jem.20190745

Figure 4. **SIRT1 modulates transcriptional regulation by NF-κB and FOXO proteins. (A)** Schematic illustration of the flow chart of RNA-seq analysis of myotubes treated with control, CM, or CM with resveratrol (Res). **(B)** Heatmap showing the Z-score changes in the three comparisons. 9 out of 101 pathways in the transcription factor database from TFactS were significantly altered. **(C)** GSEA plots of genes regulated by FOXO1 and FOXO3. The NESs for FOXO1 are 2.07 (CM treated vs. control) and −1.9 (CM + Res treated vs. CM treated) pathway. The NESs for FOXO3 are 2.5 (CM treated vs. control) and 1.6 (CM + Res treated vs. CM treated). Green line indicates enrichment profile, black vertical lines indicate hits, and gray vertical lines indicate ranking metric scores. **(D)** GSEA plots for NF-κB. NESs for NF-κB are 2.91 (CM treated vs. control) and 1.6 (CM + Res treated vs. CM treated). Green line indicates enrichment profile, black vertical lines indicate hits, and gray vertical lines indicate ranking metric scores. **(E)** mRNA levels of *Foxo1* and *Foxo3* in myotubes upon treatment with tumor cell CM and resveratrol (50 µM). **(F)** Immunoblots showing altered levels of FOXO1, FOXO3, and SIRT1 in myotubes treated with tumor cell CM and resveratrol (50 µM) for 24 h. **(G)** *Foxo1* and *Foxo3* mRNA analysis of myotubes expressing adenovirally transduced (Ad) GFP control or SIRT1 upon treatment with tumor cell CM for 24 h. **(H)** Luciferase assay to measure NF-κB–responsive promoter-luciferase reporter activity upon treatment of myotubes with cancer cell CM with and without resveratrol (50 µM) for 6 h. **(I)** Immunoblot analysis of acetylated and total p65 subunit of NF-κB in myotubes treated with cancer cell CM with and without resveratrol (50 µM) for 24 h. Data are mean ± SEM compared with one-way ANOVA with Bonferroni's multiple comparisons (E, G, and H). *, $P < 0.05$; **, $P < 0.01$; ***, $P < 0.001$. The in vitro experiments were verified in at least two independent experiments.
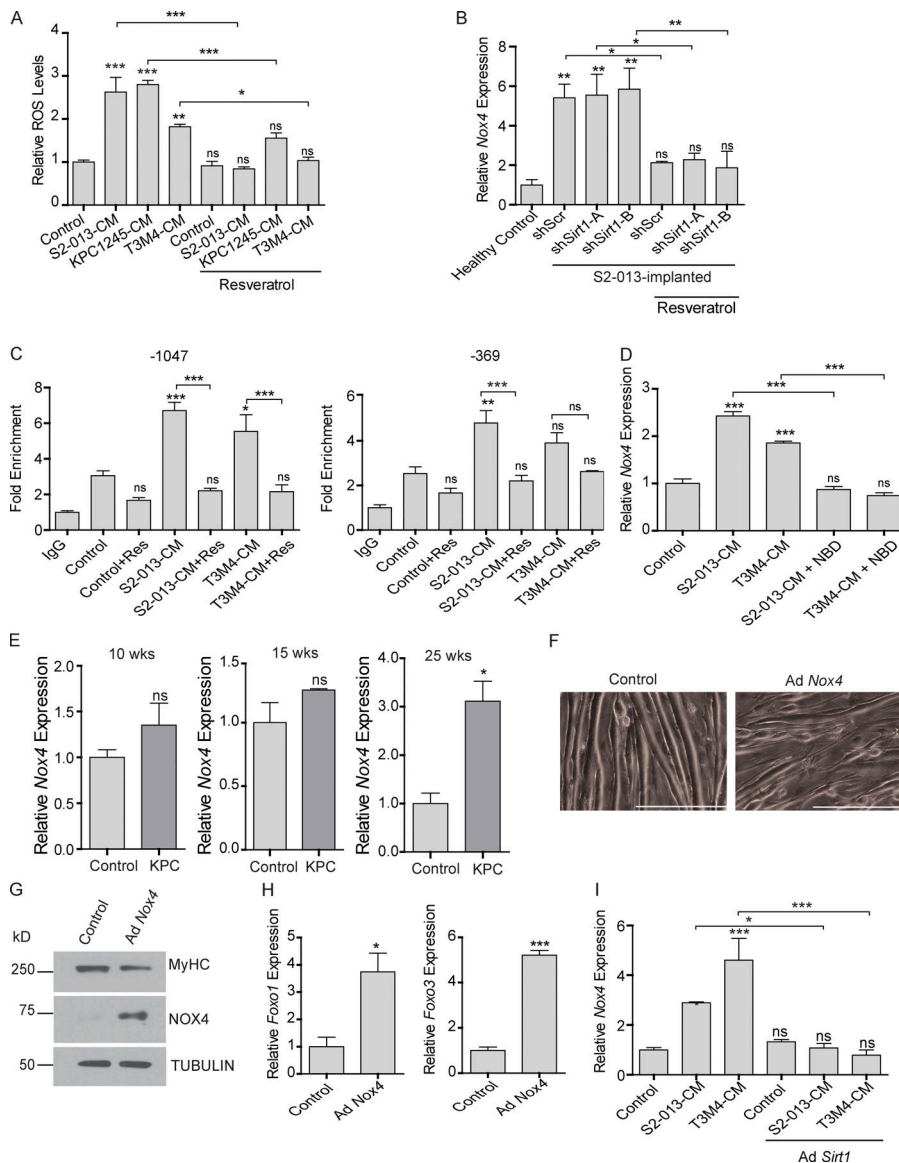
Figure 5. **SIRT1 stabilization diminishes ROS levels in cachectic muscles. (A)** ROS levels in C2C12 myotubes after treatment with cancer cell CM with or without resveratrol for 8 h. **(B)** The mRNA levels of *Nox4* in the gastrocnemius muscles from tumor cell-implanted mice (*n* = 3 for each group) with and without resveratrol treatment. **(C)** ChIP analyses demonstrating distal (−1,047) and proximal (−369) *Nox4* promoter region occupancy by NF-κB. All groups are compared with the control. **(D)** Nox4 mRNA levels in C2C12 myotubes treated with cancer cell CM and NBD. **(E)** *Nox4* mRNA levels in KPC mice muscles at 10, 15, and 25 wk of age (*n* = 3). **(F)** Brightfield microscopy images (at 200×) demonstrating thinning of the myotubes upon Nox4 overexpression. Scale bars represent 250 μm. **(G)** Immunoblot analysis of Nox4 over-expressing myotube extracts depicting decrease in the levels of myosin heavy chain. Tubulin was used as a loading control. **(H)** *Foxo1* and *Foxo3* mRNA levels in C2C12 myotubes upon *Nox4* over-expression for 48 h. **(I)** *Nox4* mRNA level in C2C12 myotubes upon treatment with cancer cell CM with or without adenoviral (Ad) expression of *Sirt1*. Data are mean ± SEM compared with one-way ANOVA with Bonferroni's multiple comparisons (A, B, C, D, and I) or Student's *t* test (E and H). *, P < 0.05; **, P < 0.01; ***, P < 0.001. In vitro experiments were verified in at least two independent experiments.

the promoter region of *Nox4* in C2C12 myotubes. We found increased occupancy of p65 at two consensus NF-κB response elements upon treatment of myotubes with S2-013- and T3M4-CM, and this promoter occupancy was reversed by resveratrol treatment (Fig. 5 C). We also used a cell permeable NF-κB essential modulator (NEMO)–binding domain (NBD) peptide that can block the activation of the IκB kinase complex and thereby inhibit NF-κB activity (Strickland and Ghosh, 2006). The NBD peptide abrogated the cancer cell CM–induced expression of *Nox4* and myotube atrophy (Fig. 5 D and Fig. S4 C).

Further supporting the role of *Nox4* in cachexia, we observed a significant increase in *Nox4* levels, along with *Foxo1, Foxo3,* MuRF1 (*Trim63*), and Atrogin-1 (*Fbxo32*) in the muscles of 25-wk-old KPC mice (Fig. 5 E) and C26 tumor-bearing mice (Fig. S4 D) compared with littermate and non–tumor-bearing controls, respectively. In agreement with these results, over-expression of *NOX4* in C2C12 myotubes via adenoviral infection led to myotube atrophy, as measured by myotube width

(Fig. 5 F), MyHC expression (Fig. 5 G), and expression of Foxo genes (Fig. 5 H). These results establish the critical role of *Nox4* in inducing the cachectic phenotype. In line with our results showing a role of SIRT1 in NOX4 regulation, over-expression of *Sirt1* was sufficient to down-regulate the cancer cell CM–induced *Nox4* expression in the myotubes treated with cancer cell CM (Fig. 5 I).

Taken together, these results can be summarized in the following model: Sirt1 down-regulation leads to NF-κB activation, which can lead to increased expression of Nox4, an inducer of oxidative stress that can in turn induce the expression of the muscle-specific ubiquitin ligases via FOXO transcription factors, to ultimately facilitate muscle atrophy (Fig. S5 A). To pharmacologically probe this pathway at each step, we used GKT137831 to inhibit Nox4 activity (Jiang et al., 2012), BMX-001 to scavenge oxygen radicals (Archambeau et al., 2013), and AS1842856 to inhibit FOXO1 activity (Zou et al., 2014). We observed that MuRF1 (*Trim63*) and Atrogin-1 (*Fbxo32*) were down-regulated by targeting all the arms of the pathway (Fig. S5 B).
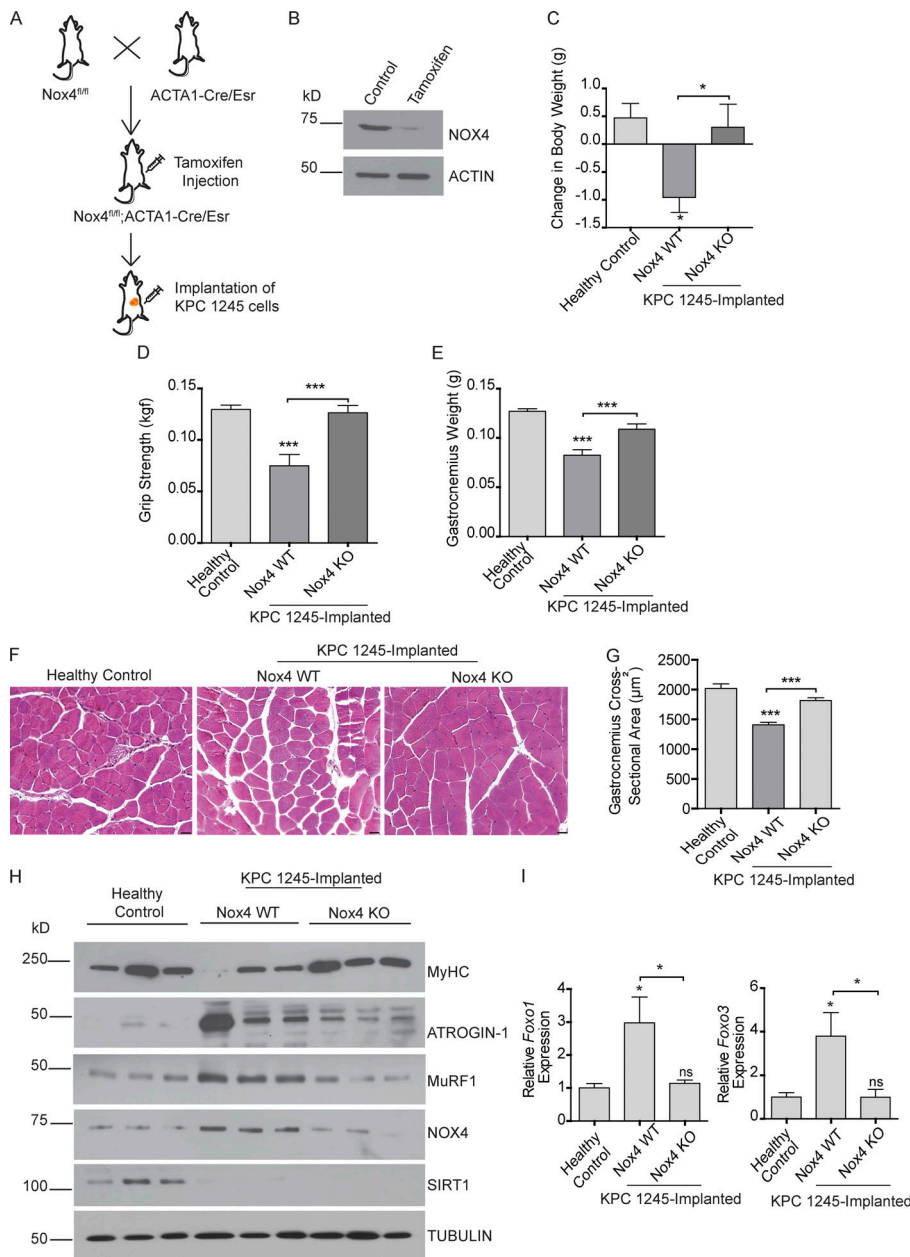
Figure 6. *Nox4* overexpression drives cachexia in orthotopic pancreatic tumor models. (A) Schematic illustration of pancreatic cancer cachexia model using *Nox4^{fl/fl}; ACTA1-cre/Esr1* mice. **(B)** Immunoblot analysis of muscle extracts from control and *Nox4* KO mice depicting deletion of Nox4 in the muscles. Actin was used as a loading control. **(C)** Change in body weight of mice after 21 d of implantation. **(D)** Grip strength of tumor-bearing *Nox4* WT and *Nox4* KO mice on day 18 after implantation. **(E)** Postnecropsy gastrocnemius muscle weight of healthy control (*n* = 10), tumor-bearing *Nox4* WT (*n* = 8), and tumor-bearing *Nox4* KO (*n* = 8) mice. **(F)** Representative hematoxylin and eosin-stained muscle sections depicting changes in the muscle fiber cross-sectional area. Scale bars represent 25 µm. **(G)** Quantification of the gastrocnemius muscle cross-sectional area of healthy controls and tumor-implanted mice (*n* = 3). **(H)** Immunoblot analyses of muscle extracts from *Nox4* WT and *Nox4* KO tumor-bearing mice. **(I)** *Foxo1* and *Foxo3* mRNA levels in gastrocnemius muscles from control and tumor-implanted mice (*n* = 5 for each group). Data are mean ± SEM compared by one-way ANOVA with Bonferroni's multiple comparisons (C–E, G, and I). *, P < 0.05; ***, P < 0.001.

Induction of Nox4 expression in skeletal muscles drives cancer-induced cachexia

To validate the cachectic role of *Nox4* in an in vivo model, we generated mice with tamoxifen-inducible conditional KO of *Nox4* in the skeletal muscles (*Nox4^{fl/fl}; ACTA1-Cre/Esr1*; Fig. 6, A and B). We then orthotopically implanted a mouse pancreatic cancer cell line (KPC1245) into the pancreas of *Nox4^{fl/fl}; ACTA1-Cre/Esr1* mice. The mice were then randomly divided into two groups to be injected with tamoxifen (*Nox4*-KO) or control solvent (*Nox4*-WT). Muscle-specific *Nox4* KO substantially ameliorated tumor-induced cachexia, as measured by body weight loss (Fig. 6 C); forelimb grip strength (Fig. 6 D); gastrocnemius muscle weight (Fig. 6 E) and cross-sectional area (Fig. 6, F and G); protein expression of MuRF1, ATROGIN-1, and myosin heavy chain (Fig. 6 H); and mRNA expression of *Foxo1* and *Foxo3* (Fig. 6 I).

Notably, there was no significant difference in tumor weights between the two groups (Fig. S5 C), suggesting that the changes in muscle/body weight and muscle function were due to muscle-intrinsic effects. *Nox4* KO did not have an impact on SIRT1 stabilization (Fig. 6 H), highlighting the importance of Nox4 as a downstream target of SIRT1. Taken together, these studies suggest that targeting Nox4 in skeletal muscle may represent a translatable strategy to treat cancer-induced cachexia.

Pharmacological inhibition of NOX4 rescues cancer cachexia in mouse models

We next investigated the anticachectic potential of GKT137831 (henceforth referred to as GKT), a NOX4/NOX1 inhibitor in phase 2 clinical trials for diabetes (NCT02010242) and primary biliary cholangitis (NCT03226067). To achieve the same, we orthotopically implanted human pancreatic cell line S2-013 in

athymic nude mice and randomly segregated them into two groups that received daily oral gavages of GKT or solvent control starting 6 d after implantation (Fig. 7 A). 3 wk after implantation, mice were sacrificed and analyzed. GKT treatment significantly diminished the S2-013 tumor-induced cachexia by all metrics that were measured, including body weight (Fig. 7 B); gastrocnemius muscle weight and fiber cross-sectional area (Fig. 7, D and H); body fat content (Fig. 7 E); grip strength (Fig. 7 F); protein expression of MuRF1, Atrogin-1, and myosin heavy chain (Fig. 7 I); and mRNA expression of Foxo1 and Foxo3 (Fig. 7 J). This correlated with a tumor-induced increase in ROS in gastrocnemius as measured by electron paramagnetic resonance (EPR) spectroscopy, which was diminished by GKT treatment (Fig. 7 G). These results were further supported by analysis of primary muscle samples from PDAC patients, which showed a significant negative correlation between myofiber cross-sectional area and NOX4 staining intensity (Fig. 7, K and L). Of note, there was no difference in tumor weight (Fig. 7 C) or muscle SIRT1 expression (Fig. 7 I) upon treatment with GKT, confirming that these effects are independent of tumor burden and downstream of SIRT1.

Cachexia is known to negatively impact patient survival; therefore, we performed survival studies in our orthotopic implantation model and observed significant survival benefit from both resveratrol and GKT treatment (Fig. S5 D). These results underscore the therapeutic potential of targeting this pathway in the setting of pancreatic cancer cachexia.

Discussion

Cancer cachexia is a known contributor to poor quality of life and mortality for cancer patients. Cancer cachexia not only contributes to overall poor prognosis but also reduces a patient's ability to tolerate chemotherapy (Aapro et al., 2014). Since there are currently no approved therapies for targeting cachexia in the clinic, our studies establish the role of the Sirt1–Nox4 axis in mediating cancer cachexia and demonstrate the utility of targeting this pathway to treat this devastating syndrome.

Our studies demonstrate that SIRT1 stabilization in the muscles successfully prevents muscle atrophy induced by pancreatic tumors in orthotopic implantation models that have been well established as models of cancer cachexia and closely resemble many aspects of the human disease (Michaelis et al., 2017; Shukla et al., 2014), such as loss in body and muscle weight. The loss of SIRT1 expression in cachectic skeletal muscle tissue was consistent across all systems examined, including a C2C12 myotube model with cancer cell CM, orthotopic implantation experiments, KPC mice with spontaneous tumors, and primary muscle tissues from human PDAC cancer patients obtained at autopsy. Abrogation of myotube thinning by exogenous expression of SIRT1 in cultures demonstrated that SIRT1 loss is the cause, not a consequence, of cancer cell CM–induced myotube wasting. Hence, our studies establish SIRT1 as a key regulator of skeletal muscle mass in the setting of cancer cachexia. While we did not observe a consistent alteration in the expression levels of other sirtuins in cachectic muscles, we cannot rule out the roles played by other sirtuins in tumor cells.

Multiple sirtuins have been shown to regulate aggressiveness in tumor cells (Kugel et al., 2016; McGlynn et al., 2015) and may indirectly impart cachectic functions. Nonetheless, our studies establish that stabilizing SIRT1 expression may be an effective therapy for cancer cachexia.

It is worth mentioning, however, that although SIRT1 stabilization provided similar survival benefit as targeting NOX4 (Fig. S5 D), some studies have suggested that SIRT1 modulation may have potential therapeutic limitations, due in part to a pro-oxidant role or tumor growth–inducing properties (de la Lastra and Villegas, 2007; San Hipólito-Luengo et al., 2017). Depending on the cellular context, SIRT1 can act either as a tumor suppressor or as a tumor promoter and may have different signaling targets in different cell types (Chen et al., 2005; Yeung et al., 2004). For example, since pancreatic tumors have high rates of glycolysis (Dang, 2010), we investigated whether resveratrol affects the glucose uptake of pancreatic cancer cells. Resveratrol decreased glucose uptake in S2-013 and T3M4 cells, an effect that was reversed by Ex-527 (Fig. S5, E and F), implying a SIRT1-dependent mechanism. Conversely, resveratrol increased glucose uptake in myotubes exposed to cancer cell CM (Fig. S5 G), highlighting the paradoxical metabolic consequences of perturbing SIRT1 in different cellular contexts. We speculate that this might be due to the differences in the expression of the glucose transporters between cancer cells and myotubes. The expression of *SLC2A1* (GLUT1) and *SLC2A4* (GLUT4) was significantly higher in the former (Fig. S5 H). Previous studies have shown that resveratrol inhibits GLUT1 in cancer cells but increases GLUT4 translocation to the membrane in myoblasts, and this differential effect might explain our result (Penumathsa et al., 2008; Zambrano et al., 2019). However, further work is warranted in this direction.

In our studies with the in vitro models of cancer cell CM–induced myodegeneration, RNA-seq analysis identified NF-κB as the most significantly altered pathway in myotubes upon CM exposure. This was in line with classical studies in cachexia that implicated NF-κB as the master regulator of ubiquitin proteasome in cancer-induced muscle atrophy (Cai et al., 2004; Han et al., 1999). Although previous studies have demonstrated an association between NF-κB activation and the proteins in the ubiquitin proteasome pathway (Cai et al., 2004; Whitehouse and Tisdale, 2003), a direct mechanism was still not known. Here, we elucidate the mechanistic regulation of muscle wasting downstream of diminished SIRT1 expression and NF-κB activation. Downstream of NF-κB activation, we observed tumor cell–induced expression of FOXO proteins, which are known to be regulated by oxidative and metabolic stress (Klotz et al., 2015). Based on the previous evidence highlighting the antioxidant functions of SIRT1 (Jang et al., 1997) and the influence of oxidative stress on muscle wasting (Ábrigo et al., 2018; Scicchitano et al., 2018), we next asked if the observed resveratrol-dependent decrease in muscle atrophy was due to altered redox balance via SIRT1-dependent attenuation of NF-κB activation. Indeed, we found that resveratrol inhibits cancer cell CM–induced activation of NF-κB and that direct inhibition of NF-κB reduces the cancer cell CM–induced expression of MuRF1 and Atrogin-1 ubiquitin ligases. This highlights the role of SIRT1 as
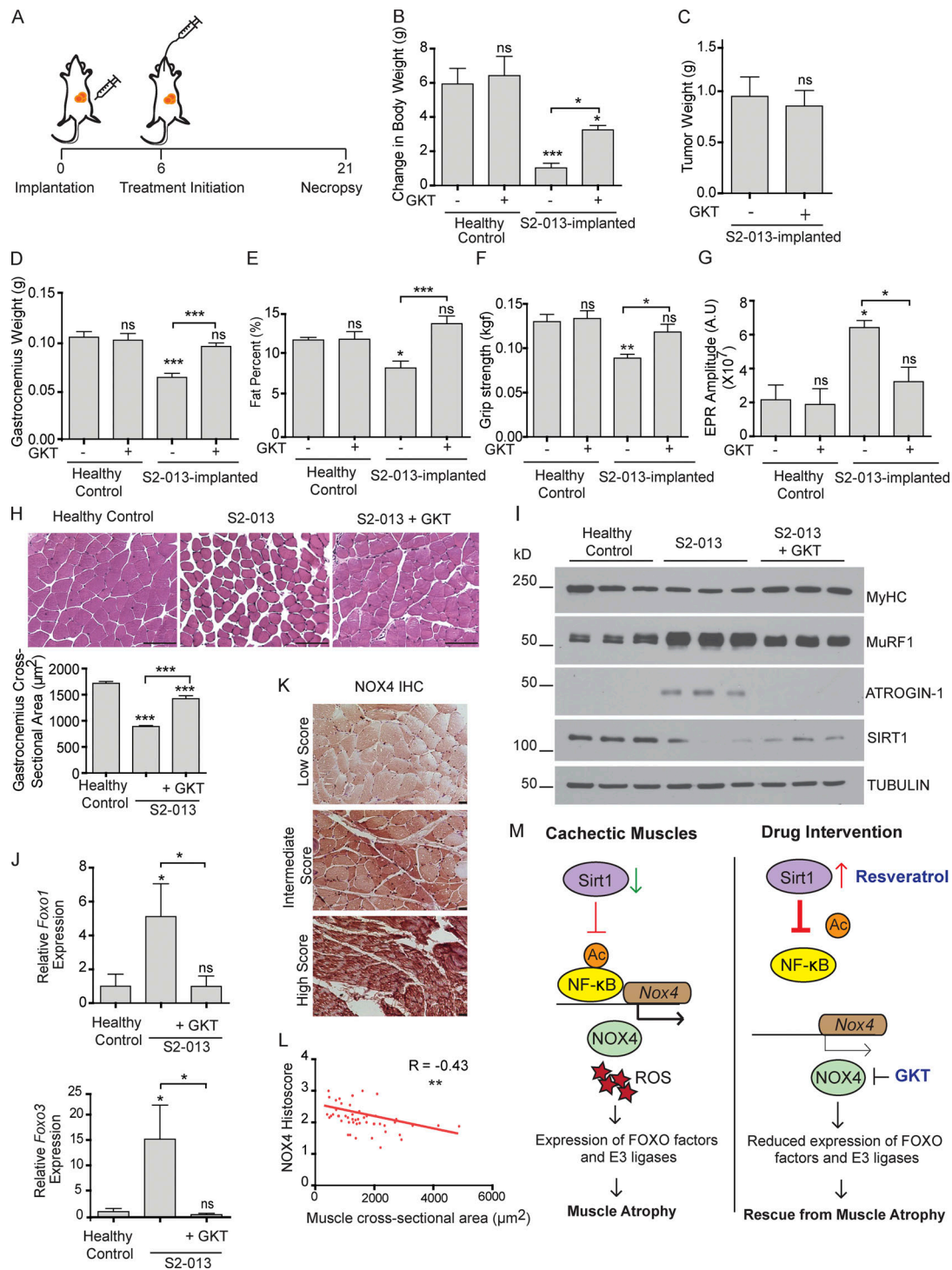
Figure 7. **Pharmacological inhibition of NOX4 rescues muscle wasting in a cancer cachexia model**. **(A)** Schematic illustration of S2-013 tumor cell implantation and GKT137831 (GKT) therapy initiation in athymic nude mice. **(B)** Change in the mouse body weight 21 d after implantation for healthy controls (*n* = 9), healthy controls with GKT (*n* = 4), S2-013 implanted (*n* = 9), and S2-013 implanted with GKT treatment (*n* = 10). **(C and D)** Postnecropsy tumor weight (C) and gastrocnemius muscle weight (D) for S2-013–implanted mice with and without GKT treatment. **(E)** Body fat percentage at day 18 in tumor-bearing mice with and without GKT treatment. **(F)** Grip strength measurements on day 18 after implantation. **(G)** Gastrocnemius muscle ROS measurement by EPR in tumor-bearing mice with and without GKT treatment (*n* = 5 for each group). **(H)** Representative images of hematoxylin and eosin–stained gastrocnemius muscle cross sections. Quantification of the cross-sectional area measured via ImageJ (*n* = 3). Scale bars represent 100 μm. **(I)** Immunoblot analysis of gastrocnemius muscle extracts from mice with indicted treatments. **(J)** *Foxo1* and *Foxo3* mRNA levels in gastrocnemius muscles from mice with indicted treatments (*n* = 3 for each group). **(K)** Representative images of NOX4-stained human muscle specimens. Scale bars represent 25 μm. **(L)** Correlation of Nox4 staining histoscore and muscle fiber cross-sectional area in skeletal muscles from human pancreatic cancer patients (*n* = 47). **(M)** Schematic illustration of the action of resveratrol and GKT as potential therapeutic interventions in combating muscle wasting in cancer. Data are mean ± SEM compared with one-way ANOVA with Bonferroni's multiple comparisons (B, D–H, and J) or Student's *t* test (C). *, P < 0.05; **, P < 0.01; ***, P < 0.001.

a key antagonist of NF-κB–induced muscle wasting and the pathophysiological importance of decreased muscle SIRT1 expression in pancreatic cancer cachexia.

Since SIRT1 is a known regulator of oxidative stress (Khan et al., 2012), we screened for redox regulators that were induced by cancer cell CM. Our screen identified Nox4 to be the key oxidative stress regulator that was induced in the muscles of tumor-bearing mice, an effect that was abolished by resveratrol treatment. While previous studies have shown that Nox4 is regulated by NF-κB in different models (Manea et al., 2010; Williams et al., 2012), we demonstrate that *Nox4* promoter occupancy by NF-κB and NF-κB activity are significantly induced by tumor cell CM, and the effect is diminished by resveratrol. Furthermore, muscle-specific *Nox4* KO and pharmacological blockade of Nox4 in tumor-bearing mice abolished tumor-induced muscle atrophy and reduced Nox4-induced *Foxo1* and *Foxo3* expression. These studies demonstrate that SIRT1 regulates oxidative stress and atrophy in skeletal muscles by NF-κB–mediated expression of *Foxo1* and *Foxo3*, via NOX4. It remains to be identified what down-regulates SIRT1 expression. Transforming growth factor β, which has been shown to induce Nox4 (Carmona-Cuenca et al., 2008), is a potential regulator. However, in our model, it failed to decrease the expression of *Sirt1* (Fig. S5 I). We speculate that the modulation of energy homeostasis and metabolism in cachectic muscles might be responsible for the alteration in Sirt1 levels.

The clinical relevance of these findings is underscored by the observed significant negative correlation of NOX4 expression with the skeletal muscle fiber cross-sectional area in human pancreatic cancer patients. NOX4 has also been reported to drive tumor progression downstream of activated KRAS (Ju et al., 2017) and promote epithelial-mesenchymal transition in pancreatic cancer cells (Hiraga et al., 2013). These findings suggest a potential dual role for NOX4 inhibition in pancreatic cancer therapy. However, we did not observe a significant reduction in tumor burden upon Nox4 inhibition via GKT. The contrasting results might be due to the inherent characteristics of the cell lines that were used or the insufficient dosage of the compound to impact tumor burden. Of note, the role of SIRT1 in cancer is ambiguous. Depending on the cellular context, SIRT1 could act either as a tumor suppressor or as a tumor promoter and may have different signaling targets in different cancer types (Chen et al., 2005; Yeung et al., 2004). These studies, along with our present study, suggest the potential of NOX4, but perhaps not the upstream signaling regulator Sirt1, as a therapeutic target for future clinical studies. Of note, the NOX4 inhibitor GKT137831 is already in clinical trials for various diseases. Interestingly, Nox4 is also up-regulated in angiotensin II–induced muscle wasting, implying the possibility of a common pathway (Kadoguchi et al., 2018) in multiple muscle disorders. Since other disorders such as muscular dystrophy also show increased muscle NF-κB or NOX4 activity (Whitehead et al., 2010), GKT could be effective in treating muscle wasting induced by a variety of pathologies, a possibility that warrants further investigation.

Overall, this study demonstrates that tumor-induced muscle wasting was mediated by the SIRT1 loss and the resulting activation of NF-κB, which in turn induces the expression of Nox4

in skeletal muscles, leading to the induction of protein degradation pathways (Fig. 7 M). These findings provide new insights into the mechanisms that underlie weight and muscle loss in cancer cachexia. These studies provide novel therapeutic opportunities for targeting tumor-induced skeletal muscle wasting.

Materials and methods

Cell culture and reagents
Pancreatic cancer cell lines T3M4 and S2-013 were generous gifts from Dr. Michael A. Hollingsworth (Eppley Institute, UNMC, Omaha, NE; Chaika et al., 2012). hTERT-HPNE (HPNE) cells were a kind gift from Dr. Michel M. Ouellette (UNMC, Omaha, NE; Lee et al., 2003). Cancer cell line C26 and HEK293T cells was obtained from ATCC. Cell lines were validated by STR profiling by the Genetics Core at University of Arizona. Mouse KPC pancreatic cancer cell lines were derived from the transgenic mouse models described below. All cell lines were cultured in DMEM (Sigma-Aldrich) with 10% FBS, 100 IU/ml penicillin, and 100 µg/ml streptomycin and incubated at 37°C in a humidified incubator with 5% CO_2. C2C12 myoblasts were purchased from ATCC and cultured in DMEM with 10% FBS until confluent. After reaching confluency, the myoblasts were differentiated in DMEM with 2% horse serum and 1 µg/ml insulin for 72 h, as previously described (Shukla et al., 2015). Resveratrol for in vitro studies was purchased from Sigma-Aldrich, and stocks were diluted in DMSO. Ex-527 was purchased from Santa Cruz Biotechnology. NBD peptide/NF-κB blocker was purchased from Enzo Life Sciences. FOXO1 inhibitor AS-1842856 and Nox4 inhibitor GKT 137831 were purchased from Cayman Chemical Company. BMX-001 was provided by Dr. Rebecca Oberley-Deegan (UNMC, Omaha, NE).

Lentivirus and adenovirus transfections
Cell transfections for producing replication-incompetent lentivirus were performed by using Turbofect from Thermo Fisher Scientific, following the manufacturer's protocol. Short hairpin RNA constructs for stable knockdown of *Sirt1* were obtained from Sigma-Aldrich. After transfection, cells were selected using puromycin. Human *NOX4* adenovirus was provided by Dr. Melissa Teoh-Fitzgerald (UNMC, Omaha, NE). GFP-expressing adenovirus was provided by Dr. Matthew Zimmerman (UNMC, Omaha, NE).

Mouse *Sirt1* adenovirus was purchased from Applied Biological Materials. C2C12 myotubes were differentiated for 48 h, and the differentiated myotubes were infected with adenovirus with a multiplicity of infection of 200.

Cancer cell CM preparation
For CM preparation, S2-013, HPNE, KPC1245, KPC1199, and T3M4 cell lines were seeded and cultured in DMEM with 10% FBS as previously described (Shukla et al., 2015). After cells became 70–80% confluent, cells were washed twice with 1× PBS and cultured in serum-free DMEM for 24 h. The media was then collected and centrifuged at 3,000 rpm for 10 min, and the supernatant was collected in a fresh tube to be either used immediately or stored at −80°C for future use. CM was prepared

from equal number of cancer cells for each cell line. CM was reconstituted with 2% horse serum 1 µg/ml insulin before treating myotubes.

Cell viability assays
Cell viability was determined by MTT assays 72 h after treatment, as described previously (Shukla et al., 2015).

RNA isolation and quantitative RT-PCR
Total RNA was extracted from cells or tissue lysates by using TRIzol reagent (Invitrogen) as previously discussed (Shukla et al., 2015). cDNA was synthesized using Verso-cDNA synthesis kit (Thermo Fisher Scientific) according to the manufacturer's protocol. Quantitative RT-PCR was performed using SYBR Green master mix (Applied Biosystems). *Actb* (codes for β-actin) was used as an internal control. Total RNA for RNA-seq analysis was isolated using RNAeasy columns (Qiagen), as per the manufacturer's protocol. Relative gene expression analysis was performed by using the ΔΔCt method, as described previously (Shukla et al., 2015). The primer sequences are provided in Table S2.

ChIP assay
The ChIP assay was performed as described previously (Shukla et al., 2017). Briefly, ChIP assays were performed by using an antibody against p65 subunit of NF-κB (clone F-6), using IgG as a control. A total of 3 µl purified chromatin for each reaction was used for quantitative PCR (qPCR) analysis. The qPCR analysis was performed by Applied Biosystems QuantStudio 5 real-time PCR system. Each reaction was performed in triplicate. The threshold cycle values obtained for each genomic region were used for further analysis. For ChIP qPCR analysis, threshold cycle values were normalized to the input control and represented as a fold increase over the enrichment detected using IgG.

Immunohistochemistry
Immunohistochemistry was performed as described previously (Shukla et al., 2015). We used Novolink Polymer (Leica), as per the manufacturer's instructions. Muscle sections prepared from human patient tissues were stained with SIRT1 antibody (Cell Signaling Technology) and NOX4 antibody (Abcam). Each muscle fiber in a cross-sectional field of view was given an intensity score by evaluating staining intensity of positive staining (0 = none, 1 = weak, 2 = intermediate, 3 = strong). The histoscore was calculated by multiplying the percentage of fibers (0–100) with the particular score by its corresponding intensity score (0–3). All the scores in a given section were added, and the value was then divided by 100 to attain a score between 1 and 3.

Immunoblotting
Protein isolation and Western blotting were performed as described previously (Shukla et al., 2015). Briefly, cells were washed twice with PBS and lysed in radioimmunoprecipitation assay lysis buffer by shaking on ice for 10 min. Then, the lysates were centrifuged at 13,000 rpm for 5 min, and the supernatant was collected. Protein concentration was measured by the Bradford assay. Equal amounts of protein were loaded into the SDS-PAGE gel for immunoblotting. Primary antibodies against MuRF1, ATROGIN-1, and p65 (NF-κB; Santa Cruz Biotechnology); SIRT1, FOXO3a, FOXO1, and Acetyl-p65 (K310; Cell Signaling Technology); tubulin, actin (JLA20), and MyHC (Developmental Studies Hybridoma Bank); and NOX4 (Abcam) were used for probing specific proteins. Loading control was run in parallel on separate gels for each experiment.

SIRT1 activity assay
SIRT1 activity was measured in myotubes b–y using a SIRT1 activity assay kit, following the manufacturer's protocol (Sigma-Aldrich). C2C12 myotubes were treated with S2-013 and T3M4 cancer cell CM for 24 h, and SIRT1 activity was measured.

NF-κB reporter assay
NF-κB luciferase adenovirus was purchased from Vector Biolabs. C2C12 cells were seeded and differentiated as previously mentioned in 6-well plates. C2C12 myotubes were then treated with cancer cell CM for 6 h with and without resveratrol. After 6 h, cells were lysed and assayed for luciferase activity using Promega Luciferase Reporter Assay according to the manufacturer's instructions.

Caspase 3/7 activity assay
C2C12 myotubes were treated with control or cancer cell CM. Caspase 3/7 activity assay was performed using Promega Caspase Glo-kit as previously described (Shukla et al., 2015).

Metabolomics of CM
Serum-free DMEM was added to HPNE and S2-013 cells, and the CM was collected after 24 h. Polar metabolites were extracted from the CM and analyzed via liquid chromatography–coupled tandem mass spectrometry as previously described (Shukla et al., 2017).

Animal studies
Orthotopic studies
All animal experiments performed in this study were approved by the UNMC Institutional Animal Care and Use Committee. Female athymic nude mice (NCr-nu/nu) were bred in-house, and 6–8-wk-old mice were used for orthotopic implantations. 0.5 × 10⁶ S2-013 scrambled control, S2-013 sh*SIRT1*-A, or S2-013 sh*SIRT1*-B cells were injected into the mouse pancreas, and 7 d after implantation, mice were randomized into groups of 10 animals each. Age- and gender-matched mice, without any tumor cell injection, were used as healthy controls. Trans-resveratrol (Cayman Chemical) was solubilized in 1.5% methylcellulose with vigorous vortexing (Shadfar et al., 2011). Beginning on day 7, mice received a daily oral gavage of 200 mg/kg trans-resveratrol delivered using a 20G gavage needle. Tumor volumes and body weights were recorded regularly. After 14 d of treatment, all mice were euthanized, and tumor weight, tumor volume, gastrocnemius muscle weight, and body weight were measured. Tumor tissue, liver, spleen, and muscles were flash frozen in liquid nitrogen and formalin fixed for further analysis.

For GKT137831 studies, 0.25 × 10⁶ S2-013 cells were implanted in the pancreas of athymic nude mice. After 7 d of

Dasgupta et al.
Targeting Sirt1–Nox4 signaling in cancer cachexia

Journal of Experimental Medicine   13 of 17
https://doi.org/10.1084/jem.20190745

implantation, the mice were randomized into two groups. GKT137831 was solubilized in 1.2% of methylcellulose and 0.1% of polysorbate 80 and administered to 10 tumor-bearing mice at a concentration of 60 mg/kg via daily oral gavage. The other mouse cohort was gavaged with the solvent solution. To test for toxicity, we also gavaged four healthy mice with GKT137831. An independent cohort of similarly treated mice were used for survival studies.

For studies with C26 cells, 0.5×10^6 cells were implanted subcutaneously in athymic nude mice. Tissues were collected 21 d after implantation.

KPC tissues
The muscles of 10-, 15-, and 25-wk-old littermate controls or mice from C57BL/6-congenic KPC spontaneous progression model of pancreatic cancer and littermate controls were harvested by euthanizing the mice at the respective ages.

Transgenic mouse model
C57BL/6 mice expressing tamoxifen-inducible muscle-specific Cre recombinase (ACTA1-cre/Esr1) were obtained from the Jackson Laboratory (McCarthy et al., 2012). Nox4-floxed mice have been described previously (Kuroda et al., 2010). These mice were crossbred to get the desired mice genotype (Nox4^{fl/fl}; ACTA1-cre/Esr1). Nox4 KO in the skeletal muscles was induced by administration of tamoxifen for 5 consecutive days at a concentration of 75 mg/kg, as suggested by the Jackson Laboratory. Littermates were used as controls for the studies.

0.25×10^5 KPC1245 cells were implanted into the pancreas of male age-matched Nox4^{fl/fl}; ACTA1-cre/Esr1 mice or littermate controls. After implantation, mice were randomized into two groups of eight mice each, and one group was injected with tamoxifen to induce Nox4 deletion in the muscles.

Mouse body fat measurement
Fat percentage in each mouse was measured by dual-energy x-ray absorptiometry scanning on the 18th day after implantation as previously described (Henry et al., 2014). Mice were anesthetized using a mixture of isoflurane and oxygen and placed on the positioning tray in the imager. Mice were scanned using a Lunar PIXImus densitometer (GE Medical-Lunar).

Patient samples
Skeletal muscle specimens (pectoral or diaphragm) collected from pancreatic cancer patients were obtained from the UNMC's Tissue Bank through the Rapid Autopsy Program for Pancreas. The tissues were harvested with appropriate consent, as approved by the UNMC Institutional Review Board under application IRB 091–01.

Measurement of grip strength
A grip strength meter (Columbus Instruments) was used to assess forelimb grip strength as previously described (Shukla et al., 2015). On the 18th day of treatment, we acclimatized mice to the procedure room for 15 min and measured grip strength as per the manufacturer's instructions.

Detection of ROS in muscles
EPR spectroscopy was used to detect oxygen radicals in the muscle tissues as previously described (Case et al., 2013). Briefly, gastrocnemius muscle tissues were harvested and incubated for 1 h at 37°C with the cell-permeable superoxide ($O_2^{\cdot-}$)-sensitive spin probe 1-hydroxy-3-methoxycarbonyl-2,2,5,5-tetramethylpyrrolidine (200 µmol/liter; Noxygen Science Transfer and Diagnostics) in a Krebs-Hepes buffer (pH 7.4) supplemented with the metal chelators diethyldithiocarbamate (5 µM) and deferoxamine (25 µM). The EPR–1-hydroxy-3-methoxycarbonyl-2,2,5,5-tetramethylpyrrolidine spectra were normalized to the gastrocnemius muscle weight.

ROS assay
ROS levels in cells were determined as described previously (Abrego et al., 2017). Briefly, ROS levels were determined by using oxidation-sensitive fluorescent dye 2′,7′–dichlorofluorescein diacetate (DCFDA). C2C12 cells were seeded at 3.0×10^4 cells per well in a clear-bottom black 96-well plate. The C2C12 myotubes were then differentiated and treated with the CM for 8 h. The medium was replaced with fresh DMEM containing 20 µM DCFDA, and cells were incubated at 37°C for 30 min. H_2O_2 along with DCFDA was used as a positive control, and 2′,7′-Bis(2-carboxyethyl)-5(6)-carboxyfluorescein was used as a negative control. The cells were washed with PBS, and DCFDA fluorescence was measured at 485-nm excitation wavelength and 529-nm emission wavelength using a BioTek Cytation 3 plate reader (BioTek Instruments).

Glucose uptake assay
Glucose uptake assay was performed as previously described (Abrego et al., 2017). Briefly, S2-013 and T3M4 cells were seeded at a density of 5×10^4 cells/well in 12-well plates. After overnight attachment, the cells were treated with resveratrol (25 µM) or Ex-527 (0.5 µM) for 24 h. The cells were then starved for 2 h in DMEM without glucose, glutamine, pyruvate, and FBS. [^{3}H]2-deoxy glucose was then added to the wells, incubated for 20 min, washed once with 1× PBS, and then lysed with 1% SDS. The lysates were then counted for tritium incorporation by a scintillation counter, which was then normalized according to cell counts. For C2C12 myotubes, glucose uptake was performed after the differentiated myotubes were treated for 24 h, and values were normalized with the respective protein content.

RNA-seq analysis
RNA-seq analysis was performed on C2C12-differentiated myotubes treated with S2-013-CM with or without resveratrol. All gene sets in GMT file format with Entrez IDs for Mus musculus were downloaded from http://ge-lab.org/gskb/. The gene set for TFactS (http://www.tfacts.org/) was chosen from the list and was made into a separate file, converted into gene symbols through Ensembl BioMart (https://www.ensembl.org/biomart/martview), and predicted genes and pseudogene were removed ($n = 10$) before being used by GSEA2 v2.2.3 with 1,000 permutations in the classic scoring scheme. A heatmap of the normalized enrichment score (NES) was produced in R v3.3.2 with the gplots package after filtering for the top 25% most variable gene sets. RNA-seq data files for one sample each of untreated

Dasgupta et al.
Targeting Sirt1–Nox4 signaling in cancer cachexia

Journal of Experimental Medicine 14 of 17
https://doi.org/10.1084/jem.20190745

C2C12 myotubes or C2C12 myotubes treated with S2-013-CM with or without resveratrol for 24 h have been submitted to GEO repository under the accession no. GSE147554.

Online supplemental material

Fig. S1 demonstrates the expression of sirtuins and cachectic markers in various cancer models, including the spontaneous progression mouse model of pancreatic cancer. Fig. S2 illustrates the expression levels of various sirtuins and metabolites depleted in the cancer cell CM and their effect on muscle wasting. Fig. S3 shows the effect of pharmacological manipulation of SIRT1 on markers of adipose tissue muscle wasting and redox regulators. Fig. S4 presents the expression levels of NOX4 and atrophy markers upon Sirt1 stabilization and NF-κB inhibition. Fig. S5 elucidates the SIRT1-NOX4 signaling cascade by using various pharmacological inhibitors of key regulators. Table S1 shows patient characteristics. Table S2 shows primer sequences used.

References

Aapro, M., J. Arends, F. Bozzetti, K. Fearon, S.M. Grunberg, J. Herrstedt, J. Hopkinson, N. Jacquelin-Ravel, A. Jatoi, S. Kaasa, et al; ESMO (European School of Medical Oncology). 2014. Early recognition of malnutrition and cachexia in the cancer patient: a position paper of a European School of Oncology Task Force. *Ann. Oncol.* 25:1492–1499. https://doi.org/10.1093/annonc/mdu085

Abrego, J., V. Gunda, E. Vernucci, S.K. Shukla, R.J. King, A. Dasgupta, G. Goode, D. Murthy, F. Yu, and P.K. Singh. 2017. GOT1-mediated anaplerotic glutamine metabolism regulates chronic acidosis stress in pancreatic cancer cells. *Cancer Lett.* 400:37–46. https://doi.org/10.1016/j.canlet.2017.04.029

Ábrigo, J., A.A. Elorza, C.A. Riedel, C. Vilos, F. Simon, D. Cabrera, L. Estrada, and C. Cabello-Verrugio. 2018. Role of Oxidative Stress as Key Regulator of Muscle Wasting during Cachexia. *Oxid. Med. Cell. Longev.* 2018. 2063179. https://doi.org/10.1155/2018/2063179

Amat, R., A. Planavila, S.L. Chen, R. Iglesias, M. Giralt, and F. Villarroya. 2009. SIRT1 controls the transcription of the peroxisome proliferator-activated receptor-gamma Co-activator-1alpha (PGC-1alpha) gene in skeletal muscle through the PGC-1alpha autoregulatory loop and interaction with MyoD. *J. Biol. Chem.* 284:21872–21880. https://doi.org/10.1074/jbc.M109.022749

Archambeau, J.O., A. Tovmasyan, R.D. Pearlstein, J.D. Crapo, and I. Batinic-Haberle. 2013. Superoxide dismutase mimic, MnTE-2-PyP(5+) ameliorates acute and chronic proctitis following focal proton irradiation of the rat rectum. *Redox Biol.* 1:599–607. https://doi.org/10.1016/j.redox.2013.10.002

Bachmann, J., M. Heiligensetzer, H. Krakowski-Roosen, M.W. Büchler, H. Friess, and M.E. Martignoni. 2008. Cachexia worsens prognosis in patients with resectable pancreatic cancer. *J. Gastrointest. Surg.* 12:1193–1201. https://doi.org/10.1007/s11605-008-0505-z

Bachmann, J., K. Ketterer, C. Marsch, K. Fechtner, H. Krakowski-Roosen, M.W. Büchler, H. Friess, and M.E. Martignoni. 2009. Pancreatic cancer related cachexia: influence on metabolism and correlation to weight loss and pulmonary function. *BMC Cancer.* 9:255. https://doi.org/10.1186/1471-2407-9-255

Baracos, V.E., L. Martin, M. Korc, D.C. Guttridge, and K.C.H. Fearon. 2018. Cancer-associated cachexia. *Nat. Rev. Dis. Primers.* 4:17105. https://doi.org/10.1038/nrdp.2017.105

Bodine, S.C., E. Latres, S. Baumhueter, V.K. Lai, L. Nunez, B.A. Clarke, W.T. Poueymirou, F.J. Panaro, E. Na, K. Dharmarajan, et al. 2001. Identification of ubiquitin ligases required for skeletal muscle atrophy. *Science.* 294:1704–1708. https://doi.org/10.1126/science.1065874

Bosch-Presegué, L., and A. Vaquero. 2011. The dual role of sirtuins in cancer. *Genes Cancer.* 2:648–662. https://doi.org/10.1177/1947601911417862

Buck, M., and M. Chojkier. 1996. Muscle wasting and dedifferentiation induced by oxidative stress in a murine model of cachexia is prevented by inhibitors of nitric oxide synthesis and antioxidants. *EMBO J.* 15:1753–1765. https://doi.org/10.1002/j.1460-2075.1996.tb00524.x

Cai, D., J.D. Frantz, N.E. Tawa, Jr., P.A. Melendez, B.C. Oh, H.G. Lidov, P.O. Hasselgren, W.R. Frontera, J. Lee, D.J. Glass, et al. 2004. IKKbeta/NF-kappaB activation causes severe muscle wasting in mice. *Cell.* 119:285–298. https://doi.org/10.1016/j.cell.2004.09.027

Carmona-Cuenca, I., C. Roncero, P. Sancho, L. Caja, N. Fausto, M. Fernández, and I. Fabregat. 2008. Upregulation of the NADPH oxidase NOX4 by TGF-beta in hepatocytes is required for its pro-apoptotic activity. *J. Hepatol.* 49:965–976. https://doi.org/10.1016/j.jhep.2008.07.021

Case, A.J., S. Li, U. Basu, J. Tian, and M.C. Zimmerman. 2013. Mitochondrial-localized NADPH oxidase 4 is a source of superoxide in angiotensin II-stimulated neurons. *Am. J. Physiol. Heart Circ. Physiol.* 305:H19–H28. https://doi.org/10.1152/ajpheart.00974.2012

Chaika, N.V., T. Gebregiworgis, M.E. Lewallen, V. Purohit, P. Radhakrishnan, X. Liu, B. Zhang, K. Mehla, R.B. Brown, T. Caffrey, et al. 2012. MUC1 mucin stabilizes and activates hypoxia-inducible factor 1 alpha to

regulate metabolism in pancreatic cancer. *Proc. Natl. Acad. Sci. USA.* 109: 13787–13792. https://doi.org/10.1073/pnas.1203339109

Chen, L.F., Y. Mu, and W.C. Greene. 2002. Acetylation of RelA at discrete sites regulates distinct nuclear functions of NF-kappaB. *EMBO J.* 21: 6539–6548. https://doi.org/10.1093/emboj/cdf660

Chen, W.Y., D.H. Wang, R.C. Yen, J. Luo, W. Gu, and S.B. Baylin. 2005. Tumor suppressor HIC1 directly regulates SIRT1 to modulate p53-dependent DNA-damage responses. *Cell.* 123:437–448. https://doi.org/10.1016/j.cell.2005.08.011

Chen, Y., H. Liu, H. Zhang, E. Liu, C.B. Xu, and X. Su. 2016. The sirt1/NF-kB signaling pathway is involved in regulation of endothelin type B receptors mediated by homocysteine in vascular smooth muscle cells. *Biomed. Pharmacother.* 84:1979–1985. https://doi.org/10.1016/j.biopha.2016.11.011

Dang, C.V.. 2010. Rethinking the Warburg effect with Myc micromanaging glutamine metabolism. *Cancer Res.* 70:859–862. https://doi.org/10.1158/0008-5472.CAN-09-3556

de la Lastra, C.A., and I. Villegas. 2007. Resveratrol as an antioxidant and pro-oxidant agent: mechanisms and clinical implications. *Biochem. Soc. Trans.* 35:1156–1160. https://doi.org/10.1042/BST0351156

Dewys, W.D., C. Begg, P.T. Lavin, P.R. Band, J.M. Bennett, J.R. Bertino, M.H. Cohen, H.O. Douglass, Jr., P.F. Engstrom, E.Z. Ezdinli, et al; Eastern Cooperative Oncology Group. 1980. Prognostic effect of weight loss prior to chemotherapy in cancer patients. *Am. J. Med.* 69:491–497. https://doi.org/10.1016/S0149-2918(05)80001-3

Dong, W., X. Wang, S. Bi, Z. Pan, S. Liu, H. Yu, H. Lu, X. Lin, X. Wang, T. Ma, et al. 2014. Inhibitory effects of resveratrol on foam cell formation are mediated through monocyte chemotactic protein-1 and lipid metabolism-related proteins. *Int. J. Mol. Med.* 33:1161–1168. https://doi.org/10.3892/ijmm.2014.1680

Ebrahimi, B., S.L. Tucker, D. Li, J.L. Abbruzzese, and R. Kurzrock. 2004. Cytokines in pancreatic carcinoma: correlation with phenotypic characteristics and prognosis. *Cancer.* 101:2727–2736. https://doi.org/10.1002/cncr.20672

Fearon, K.C., A.C. Voss, and D.S. Hustead; Cancer Cachexia Study Group. 2006. Definition of cancer cachexia: effect of weight loss, reduced food intake, and systemic inflammation on functional status and prognosis. *Am. J. Clin. Nutr.* 83:1345–1350. https://doi.org/10.1093/ajcn/83.6.1345

Fearon, K., F. Strasser, S.D. Anker, I. Bosaeus, E. Bruera, R.L. Fainsinger, A. Jatoi, C. Loprinzi, N. MacDonald, G. Mantovani, et al. 2011. Definition and classification of cancer cachexia: an international consensus. *Lancet Oncol.* 12:489–495. https://doi.org/10.1016/S1470-2045(10)70218-7

Fulco, M., R.L. Schiltz, S. Iezzi, M.T. King, P. Zhao, Y. Kashiwaya, E. Hoffman, R.L. Veech, and V. Sartorelli. 2003. Sir2 regulates skeletal muscle differentiation as a potential sensor of the redox state. *Mol. Cell.* 12:51–62. https://doi.org/10.1016/S1097-2765(03)00226-0

Fulco, M., Y. Cen, P. Zhao, E.P. Hoffman, M.W. McBurney, A.A. Sauve, and V. Sartorelli. 2008. Glucose restriction inhibits skeletal myoblast differentiation by activating SIRT1 through AMPK-mediated regulation of Nampt. *Dev. Cell.* 14:661–673. https://doi.org/10.1016/j.devcel.2008.02.004

German, N.J., and M.C. Haigis. 2015. Sirtuins and the Metabolic Hurdles in Cancer. *Curr. Biol.* 25:R569–R583. https://doi.org/10.1016/j.cub.2015.05.012

Ghisays, F., C.S. Brace, S.M. Yackly, H.J. Kwon, K.F. Mills, E. Kashentseva, I.P. Dmitriev, D.T. Curiel, S.I. Imai, and T. Ellenberger. 2015. The N-Terminal Domain of SIRT1 Is a Positive Regulator of Endogenous SIRT1-Dependent Deacetylation and Transcriptional Outputs. *Cell Rep.* 10:1665–1673. https://doi.org/10.1016/j.celrep.2015.02.036

Gomes, M.D., S.H. Lecker, R.T. Jagoe, A. Navon, and A.L. Goldberg. 2001. Atrogin-1, a muscle-specific F-box protein highly expressed during muscle atrophy. *Proc. Natl. Acad. Sci. USA.* 98:14440–14445. https://doi.org/10.1073/pnas.251541198

Gomes-Marcondes, M.C., and M.J. Tisdale. 2002. Induction of protein catabolism and the ubiquitin-proteasome pathway by mild oxidative stress. *Cancer Lett.* 180:69–74. https://doi.org/10.1016/S0304-3835(02)00006-X

Han, Y., S. Weinman, I. Boldogh, R.K. Walker, and A.R. Brasier. 1999. Tumor necrosis factor-alpha-inducible IkappaBalpha proteolysis mediated by cytosolic m-calpain. A mechanism parallel to the ubiquitin-proteasome pathway for nuclear factor-kappab activation. *J. Biol. Chem.* 274:787–794. https://doi.org/10.1074/jbc.274.2.787

Henry, M.D., D.L. Costanzo-Garvey, P.J. Klutho, and R.E. Lewis. 2014. Obesity-dependent dysregulation of glucose homeostasis in kinase suppressor of ras 2-/- mice. *Physiol. Rep.* 2. e12053. https://doi.org/10.14814/phy2.12053

Hiraga, R., M. Kato, S. Miyagawa, and T. Kamata. 2013. Nox4-derived ROS signaling contributes to TGF-β-induced epithelial-mesenchymal transition in pancreatic cancer cells. *Anticancer Res.* 33:4431–4438.

Howitz, K.T., K.J. Bitterman, H.Y. Cohen, D.W. Lamming, S. Lavu, J.G. Wood, R.E. Zipkin, P. Chung, A. Kisielewski, L.L. Zhang, et al. 2003. Small molecule activators of sirtuins extend Saccharomyces cerevisiae lifespan. *Nature.* 425:191–196. https://doi.org/10.1038/nature01960

Imai, S.I., and L. Guarente. 2016. It takes two to tango: NAD⁺ and sirtuins in aging/longevity control. *NPJ Aging Mech. Dis.* 2:16017. https://doi.org/10.1038/npjamd.2016.17

Imai, S., C.M. Armstrong, M. Kaeberlein, and L. Guarente. 2000. Transcriptional silencing and longevity protein Sir2 is an NAD-dependent histone deacetylase. *Nature.* 403:795–800. https://doi.org/10.1038/35001622

Jang, M., L. Cai, G.O. Udeani, K.V. Slowing, C.F. Thomas, C.W. Beecher, H.H. Fong, N.R. Farnsworth, A.D. Kinghorn, R.G. Mehta, et al. 1997. Cancer chemopreventive activity of resveratrol, a natural product derived from grapes. *Science.* 275:218–220. https://doi.org/10.1126/science.275.5297.218

Jiang, J.X., X. Chen, N. Serizawa, C. Szyndralewiez, P. Page, K. Schröder, R.P. Brandes, S. Devaraj, and N.J. Török. 2012. Liver fibrosis and hepatocyte apoptosis are attenuated by GKT137831, a novel NOX4/NOX1 inhibitor in vivo. *Free Radic. Biol. Med.* 53:289–296. https://doi.org/10.1016/j.freeradbiomed.2012.05.007

Ju, H.Q., H. Ying, T. Tian, J. Ling, J. Fu, Y. Lu, M. Wu, L. Yang, A. Achreja, G. Chen, et al. 2017. Mutant Kras- and p16-regulated NOX4 activation overcomes metabolic checkpoints in development of pancreatic ductal adenocarcinoma. *Nat. Commun.* 8:14437. https://doi.org/10.1038/ncomms14437

Kadoguchi, T., K. Shimada, H. Koide, T. Miyazaki, T. Shiozawa, S. Takahashi, T. Aikawa, S. Ouchi, K. Kitamura, Y. Sugita, et al. 2018. Possible Role of NADPH Oxidase 4 in Angiotensin II-Induced Muscle Wasting in Mice. *Front. Physiol.* 9:340. https://doi.org/10.3389/fphys.2018.00340

Kauppinen, A., T. Suuronen, J. Ojala, K. Kaarniranta, and A. Salminen. 2013. Antagonistic crosstalk between NF-κB and SIRT1 in the regulation of inflammation and metabolic disorders. *Cell. Signal.* 25:1939–1948. https://doi.org/10.1016/j.cellsig.2013.06.007

Khan, R.S., Z. Fonseca-Kelly, C. Callinan, L. Zuo, M.M. Sachdeva, and K.S. Shindler. 2012. SIRT1 activating compounds reduce oxidative stress and prevent cell death in neuronal cells. *Front. Cell. Neurosci.* 6:63. https://doi.org/10.3389/fncel.2012.00063

Klotz, L.O., C. Sánchez-Ramos, I. Prieto-Arroyo, P. Urbánek, H. Steinbrenner, and M. Monsalve. 2015. Redox regulation of FoxO transcription factors. *Redox Biol.* 6:51–72. https://doi.org/10.1016/j.redox.2015.06.019

Kugel, S., C. Sebastián, J. Fitamant, K.N. Ross, S.K. Saha, E. Jain, A. Gladden, K.S. Arora, Y. Kato, M.N. Rivera, et al. 2016. SIRT6 Suppresses Pancreatic Cancer through Control of Lin28b. *Cell.* 165:1401–1415. https://doi.org/10.1016/j.cell.2016.04.033

Kuroda, J., T. Ago, S. Matsushima, P. Zhai, M.D. Schneider, and J. Sadoshima. 2010. NADPH oxidase 4 (Nox4) is a major source of oxidative stress in the failing heart. *Proc. Natl. Acad. Sci. USA.* 107:15565–15570. https://doi.org/10.1073/pnas.1002178107

Lagouge, M., C. Argmann, Z. Gerhart-Hines, H. Meziane, C. Lerin, F. Daussin, N. Messadeq, J. Milne, P. Lambert, P. Elliott, et al. 2006. Resveratrol improves mitochondrial function and protects against metabolic disease by activating SIRT1 and PGC-1alpha. *Cell.* 127:1109–1122. https://doi.org/10.1016/j.cell.2006.11.013

Lee, D., and A.L. Goldberg. 2013. SIRT1 protein, by blocking the activities of transcription factors FoxO1 and FoxO3, inhibits muscle atrophy and promotes muscle growth. *J. Biol. Chem.* 288:30515–30526. https://doi.org/10.1074/jbc.M113.489716

Lee, K.M., C. Nguyen, A.B. Ulrich, P.M. Pour, and M.M. Ouellette. 2003. Immortalization with telomerase of the Nestin-positive cells of the human pancreas. *Biochem. Biophys. Res. Commun.* 301:1038–1044. https://doi.org/10.1016/S0006-291X(03)00086-X

Mammucari, C., G. Milan, V. Romanello, E. Masiero, R. Rudolf, P. Del Piccolo, S.J. Burden, R. Di Lisi, C. Sandri, J. Zhao, et al. 2007. FoxO3 controls autophagy in skeletal muscle in vivo. *Cell Metab.* 6:458–471. https://doi.org/10.1016/j.cmet.2007.11.001

Manea, A., L.I. Tanase, M. Raicu, and M. Simionescu. 2010. Transcriptional regulation of NADPH oxidase isoforms, Nox1 and Nox4, by nuclear factor-kappaB in human aortic smooth muscle cells. *Biochem. Biophys. Res. Commun.* 396:901–907. https://doi.org/10.1016/j.bbrc.2010.05.019

McCarthy, J.J., R. Srikuea, T.J. Kirby, C.A. Peterson, and K.A. Esser. 2012. Inducible Cre transgenic mouse strain for skeletal muscle-specific gene targeting. *Skelet. Muscle.* 2:8. https://doi.org/10.1186/2044-5040-2-8

McGlynn, L.M., S. McCluney, N.B. Jamieson, J. Thomson, A.I. MacDonald, K. Oien, E.J. Dickson, C.R. Carter, C.J. McKay, and P.G. Shiels. 2015. SIRT3 & SIRT7: Potential Novel Biomarkers for Determining Outcome in

Pancreatic Cancer Patients. *PLoS One*. 10. e0131344. https://doi.org/10.1371/journal.pone.0131344

Michaelis, K.A., X. Zhu, K.G. Burfeind, S.M. Krasnow, P.R. Levasseur, T.K. Morgan, and D.L. Marks. 2017. Establishment and characterization of a novel murine model of pancreatic cancer cachexia. *J. Cachexia Sarcopenia Muscle*. 8:824–838. https://doi.org/10.1002/jcsm.12225

Musarò, A., S. Fulle, and G. Fanò. 2010. Oxidative stress and muscle homeostasis. *Curr. Opin. Clin. Nutr. Metab. Care*. 13:236–242. https://doi.org/10.1097/MCO.0b013e3283368188

Oon, C.E., C. Strell, K.Y. Yeong, A. Östman, and J. Prakash. 2015. SIRT1 inhibition in pancreatic cancer models: contrasting effects in vitro and in vivo. *Eur. J. Pharmacol*. 757:59–67. https://doi.org/10.1016/j.ejphar.2015.03.064

Pardo, P.S., and A.M. Boriek. 2011. The physiological roles of Sirt1 in skeletal muscle. *Aging (Albany NY)*. 3:430–437. https://doi.org/10.18632/aging.100312

Penumathsa, S.V., M. Thirunavukkarasu, L. Zhan, G. Maulik, V.P. Menon, D. Bagchi, and N. Maulik. 2008. Resveratrol enhances GLUT-4 translocation to the caveolar lipid raft fractions through AMPK/Akt/eNOS signalling pathway in diabetic myocardium. *J. Cell. Mol. Med*. 12(6A, 6A): 2350–2361. https://doi.org/10.1111/j.1582-4934.2008.00251.x

Rathbone, C.R., F.W. Booth, and S.J. Lees. 2009. Sirt1 increases skeletal muscle precursor cell proliferation. *Eur. J. Cell Biol*. 88:35–44. https://doi.org/10.1016/j.ejcb.2008.08.003

Reed, S.A., P.B. Sandesara, S.M. Senf, and A.R. Judge. 2012. Inhibition of FoxO transcriptional activity prevents muscle fiber atrophy during cachexia and induces hypertrophy. *FASEB J*. 26:987–1000. https://doi.org/10.1096/fj.11-189977

Salminen, A., K. Kaarniranta, and A. Kauppinen. 2013. Crosstalk between Oxidative Stress and SIRT1: Impact on the Aging Process. *Int. J. Mol. Sci*. 14:3834–3859. https://doi.org/10.3390/ijms14023834

San Hipólito-Luengo, Á., A. Alcaide, M. Ramos-González, E. Cercas, S. Vallejo, A. Romero, E. Talero, C.F. Sánchez-Ferrer, V. Motilva, and C. Peiró. 2017. Dual Effects of Resveratrol on Cell Death and Proliferation of Colon Cancer Cells. *Nutr. Cancer*. 69:1019–1027. https://doi.org/10.1080/01635581.2017.1359309

Sandri, M., C. Sandri, A. Gilbert, C. Skurk, E. Calabria, A. Picard, K. Walsh, S. Schiaffino, S.H. Lecker, and A.L. Goldberg. 2004. Foxo transcription factors induce the atrophy-related ubiquitin ligase atrogin-1 and cause skeletal muscle atrophy. *Cell*. 117:399–412. https://doi.org/10.1016/S0092-8674(04)00400-3

Scicchitano, B.M., L. Pelosi, G. Sica, and A. Musarò. 2018. The physiopathologic role of oxidative stress in skeletal muscle. *Mech. Ageing Dev*. 170: 37–44. https://doi.org/10.1016/j.mad.2017.08.009

Shadfar, S., M.E. Couch, K.A. McKinney, L.J. Weinstein, X. Yin, J.E. Rodríguez, D.C. Guttridge, and M. Willis. 2011. Oral resveratrol therapy inhibits cancer-induced skeletal muscle and cardiac atrophy in vivo. *Nutr. Cancer*. 63:749–762. https://doi.org/10.1080/01635581.2011.563032

Sharples, A.P., D.C. Hughes, C.S. Deane, A. Saini, C. Selman, and C.E. Stewart. 2015. Longevity and skeletal muscle mass: the role of IGF signalling, the sirtuins, dietary restriction and protein intake. *Aging Cell*. 14:511–523. https://doi.org/10.1111/acel.12342

Shukla, S.K., T. Gebregiworgis, V. Purohit, N.V. Chaika, V. Gunda, P. Radhakrishnan, K. Mehla, I.I. Pipinos, R. Powers, F. Yu, et al. 2014. Metabolic reprogramming induced by ketone bodies diminishes pancreatic cancer cachexia. *Cancer Metab*. 2:18. https://doi.org/10.1186/2049-3002-2-18

Shukla, S.K., A. Dasgupta, K. Mehla, V. Gunda, E. Vernucci, J. Souchek, G. Goode, R. King, A. Mishra, I. Rai, et al. 2015. Silibinin-mediated metabolic reprogramming attenuates pancreatic cancer-induced cachexia and tumor growth. *Oncotarget*. 6:41146–41161. https://doi.org/10.18632/oncotarget.5843

Shukla, S.K., V. Purohit, K. Mehla, V. Gunda, N.V. Chaika, E. Vernucci, R.J. King, J. Abrego, G.D. Goode, A. Dasgupta, et al. 2017. MUC1 and HIF-1alpha Signaling Crosstalk Induces Anabolic Glucose Metabolism to Impart Gemcitabine Resistance to Pancreatic Cancer. *Cancer Cell*. 32: 71–87.e7. https://doi.org/10.1016/j.ccell.2017.06.004

Strickland, I., and S. Ghosh. 2006. Use of cell permeable NBD peptides for suppression of inflammation. *Ann. Rheum. Dis*. 65(Suppl 3):iii75-iii82. https://doi.org/10.1136/ard.2006.058438

Tissenbaum, H.A., and L. Guarente. 2001. Increased dosage of a sir-2 gene extends lifespan in Caenorhabditis elegans. *Nature*. 410:227–230. https://doi.org/10.1038/35065638

Vinciguerra, M., M. Fulco, A. Ladurner, V. Sartorelli, and N. Rosenthal. 2010. SirT1 in muscle physiology and disease: lessons from mouse models. *Dis. Model. Mech*. 3:298–303. https://doi.org/10.1242/dmm.004655

Whitehead, N.P., E.W. Yeung, S.C. Froehner, and D.G. Allen. 2010. Skeletal muscle NADPH oxidase is increased and triggers stretch-induced damage in the mdx mouse. *PLoS One*. 5. e15354. https://doi.org/10.1371/journal.pone.0015354

Whitehouse, A.S., and M.J. Tisdale. 2003. Increased expression of the ubiquitin-proteasome pathway in murine myotubes by proteolysis-inducing factor (PIF) is associated with activation of the transcription factor NF-kappaB. *Br. J. Cancer*. 89:1116–1122. https://doi.org/10.1038/sj.bjc.6601132

Williams, C.R., X. Lu, R.L. Sutliff, and C.M. Hart. 2012. Rosiglitazone attenuates NF-κB-mediated Nox4 upregulation in hyperglycemia-activated endothelial cells. *Am. J. Physiol. Cell Physiol*. 303:C213–C223. https://doi.org/10.1152/ajpcell.00227.2011

Wu, J.W., J.J. Wang, J.B. Chen, Y.L. Huang, H. Wang, G.H. Liu, L.F. Li, M. Kang, X.G. Wang, and H.H. Cai. 2015. Resveratrol could reverse the expression of SIRT1 and MMP-1 in vitro. *Genet. Mol. Res*. 14:12386–12393. https://doi.org/10.4238/2015.October.16.5

Xu, Q., L. Zong, X. Chen, Z. Jiang, L. Nan, J. Li, W. Duan, J. Lei, L. Zhang, J. Ma, et al. 2015. Resveratrol in the treatment of pancreatic cancer. *Ann. N. Y. Acad. Sci*. 1348:10–19. https://doi.org/10.1111/nyas.12837

Yang, Y., H. Hou, E.M. Haller, S.V. Nicosia, and W. Bai. 2005. Suppression of FOXO1 activity by FHL2 through SIRT1-mediated deacetylation. *EMBO J*. 24:1021–1032. https://doi.org/10.1038/sj.emboj.7600570

Yang, L., L. Yang, W. Tian, J. Li, J. Liu, M. Zhu, Y. Zhang, Y. Yang, F. Liu, Q. Zhang, et al. 2014. Resveratrol plays dual roles in pancreatic cancer cells. *J. Cancer Res. Clin. Oncol*. 140:749–755. https://doi.org/10.1007/s00432-014-1624-4

Yeung, F., J.E. Hoberg, C.S. Ramsey, M.D. Keller, D.R. Jones, R.A. Frye, and M.W. Mayo. 2004. Modulation of NF-kappaB-dependent transcription and cell survival by the SIRT1 deacetylase. *EMBO J*. 23:2369–2380. https://doi.org/10.1038/sj.emboj.7600244

Zambrano, A., M. Molt, E. Uribe, and M. Salas. 2019. Glut 1 in Cancer Cells and the Inhibitory Action of Resveratrol as A Potential Therapeutic Strategy. *Int. J. Mol. Sci*. 20:3374. https://doi.org/10.3390/ijms20133374

Zhang, W., Q. Huang, Z. Zeng, J. Wu, Y. Zhang, and Z. Chen. 2017. Sirt1 Inhibits Oxidative Stress in Vascular Endothelial Cells. *Oxid. Med. Cell. Longev*. 2017. 7543973. https://doi.org/10.1155/2017/7543973

Zhao, J., J.J. Brault, A. Schild, P. Cao, M. Sandri, S. Schiaffino, S.H. Lecker, and A.L. Goldberg. 2007. FoxO3 coordinately activates protein degradation by the autophagic/lysosomal and proteasomal pathways in atrophying muscle cells. *Cell Metab*. 6:472–483. https://doi.org/10.1016/j.cmet.2007.11.004

Zhou, J.H., H.Y. Cheng, Z.Q. Yu, D.W. He, Z. Pan, and D.T. Yang. 2011. Resveratrol induces apoptosis in pancreatic cancer cells. *Chin. Med. J. (Engl.)*. 124:1695–1699.

Zou, P., L. Liu, L. Zheng, L. Liu, R.E. Stoneman, A. Cho, A. Emery, E.R. Gilbert, and Z. Cheng. 2014. Targeting FoxO1 with AS1842856 suppresses adipogenesis. *Cell Cycle*. 13:3759–3767. https://doi.org/10.4161/15384101.2014.965977
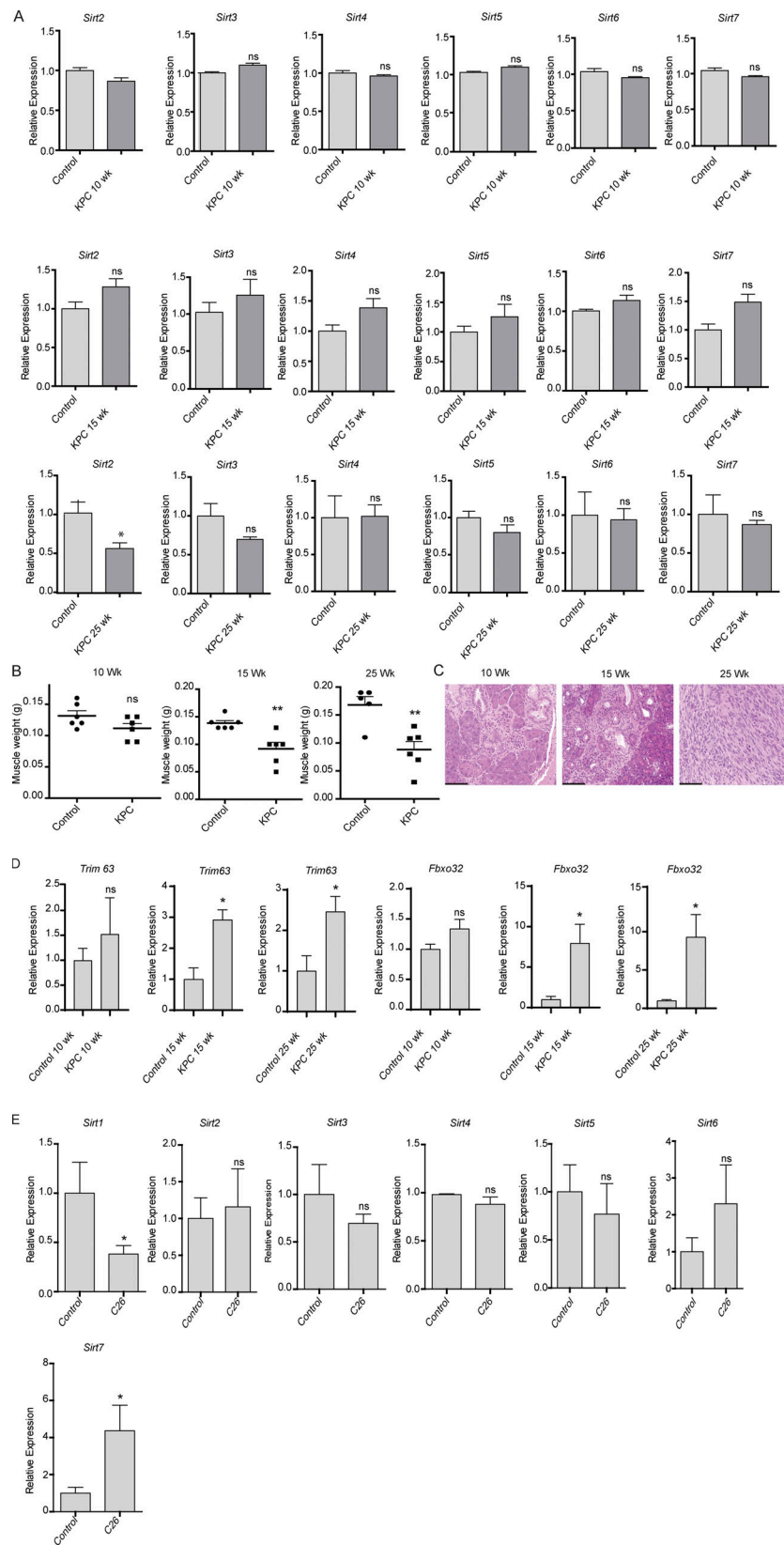
Supplemental material

Figure S1. **Muscle wasting with disease progression in KPC mice and colon cancer cachexia model. (A)** Sirtuin mRNA expression in gastrocnemius muscles from KPC mice at 10, 15, and 25 wk of age. **(B)** Gastrocnemius muscle weights and (C) hematoxylin and eosin–stained pancreas sections of control and KPC mice at 10, 15, and 25 wk of age, (D) mRNA expression of *Trim63* and *Fbxo32* in muscles of control and KPC mice at 10, 15, and 25 wk of age. **(E)** Sirtuin mRNA expression in gastrocnemius muscles from C26 tumor-bearing mice at 21 d after implantation (*n* = 5 in each group). Scale bars represent 93.4 μm. Data are mean ± SEM compared with Student's *t* test. *, P < 0.05; **, P < 0.01.
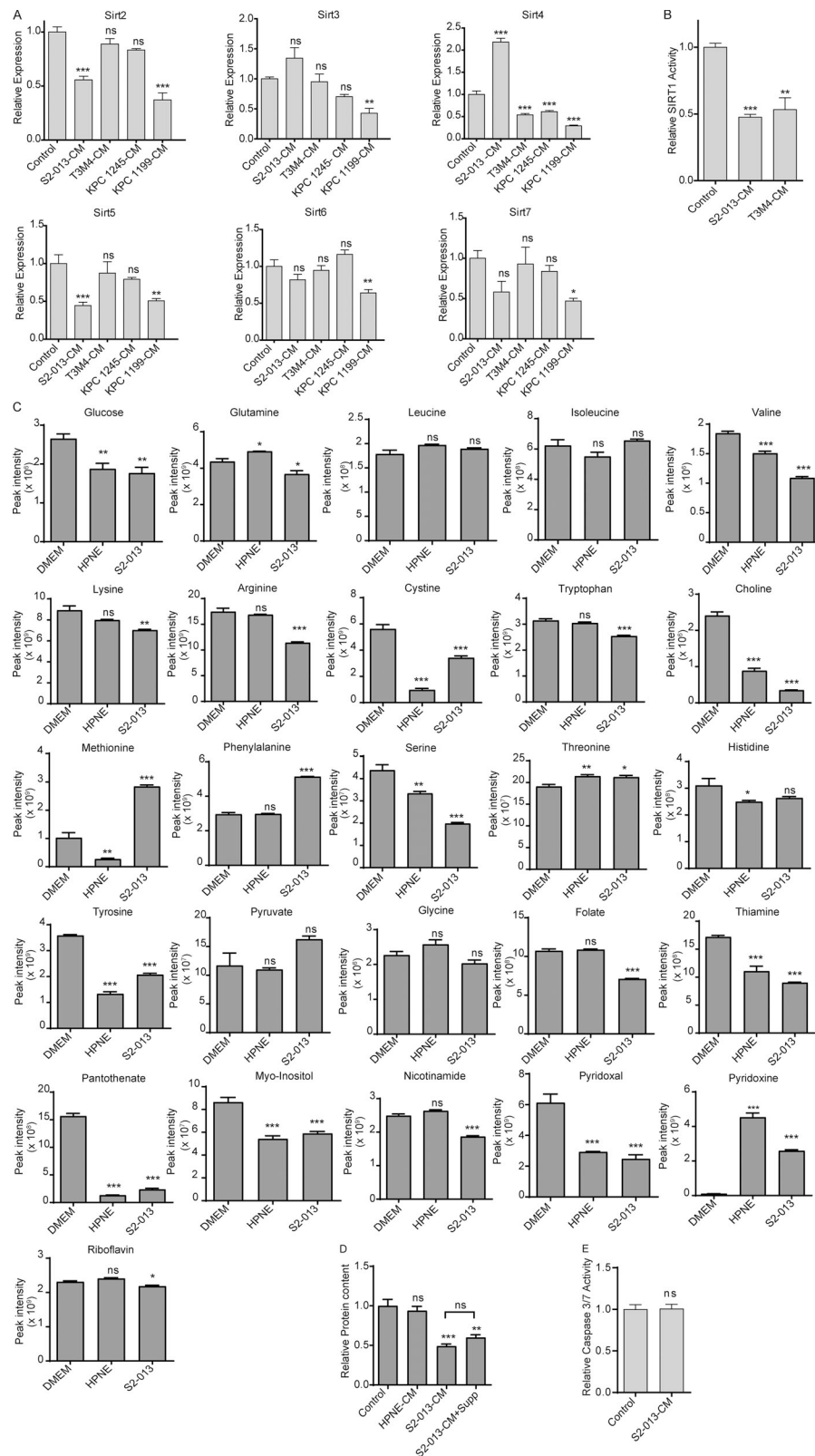
Figure S2. **In vitro characterization of sirtuins and metabolite abundance. (A)** *Sirt2*, *Sirt3*, *Sirt4*, *Sirt5*, *Sirt6*, and *Sirt7* mRNA expression in control myotubes and myotubes treated with S2-013, T3M4, KPC1245, and KPC1199 CM for 24 h. **(B)** Sirt1 activity in control myotubes and myotubes treated with S2-013 and T3M4 CM for 24 h. **(C)** Relative metabolite levels in DMEM and HPNE and S2-013 CM. **(D)** Relative protein content of C2C12 myotubes treated with DMEM and HPNE CM, S2-013 CM, and S2-013 CM + supplements (Supp; metabolites that decreased >25% in S2-013 CM relative to DMEM). **(E)** Caspase 3/7 activity in control and cancer cell CM–treated C2C12 myotubes. Data are mean ± SEM compared with one-way ANOVA with Dunnett's (A–D) multiple comparisons and Student's *t* test (E). *, P < 0.05; **, P < 0.01; ***, P < 0.001. In vitro experiments were verified in at least two independent experiments.
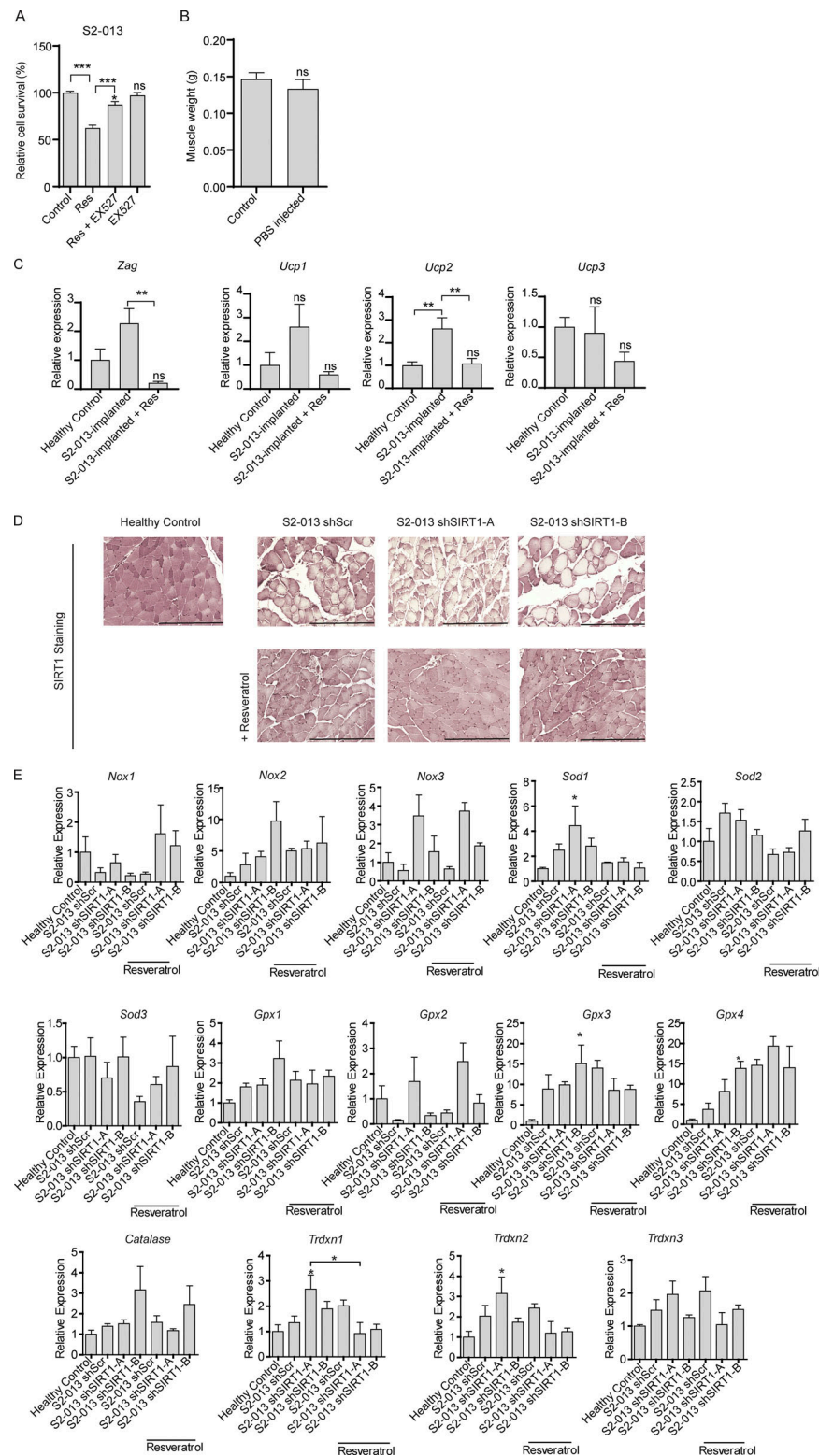
Figure S3. **Effect of SIRT1 manipulation in cancer cells on adipose tissue muscle wasting and redox regulators. (A)** Cell survival assay of S2-013 cells treated with resveratrol (50 µM), Ex-527 (0.1 µM), or both for 72 h. **(B)** Gastrocnemius muscle weight of control and PBS-injected mice. **(C)** Relative mRNA levels of *Zag* (Zinc α2-glycoprotein) and *Ucp 1-3* in adipose tissues of tumor-bearing mice with and without resveratrol treatment. **(D)** SIRT1 staining in gastrocnemius muscles of healthy controls and tumor-bearing mice treated with vehicle control or resveratrol. Scale bars represent 250 µm. **(E)** The mRNA levels of redox regulators in gastrocnemius muscles of tumor-bearing mice with and without resveratrol treatment (*n* = 3 for each group): *Nox1–Nox3*, superoxide dismutase 1–3 (*Sod1–Sod3*), glutathione peroxidase 1–4 (*Gpx1–Gpx4*), *Catalase*, and thioredoxin 1–3 (*Trdxn1–Trdxn3*). Data are mean ± SEM compared with one-way ANOVA with Bonferroni's (A, C, and E) multiple comparisons or Student's *t* test (B). *, $P < 0.05$, **, $P < 0.01$; ***, $P < 0.001$. In vitro experiments were verified in at least two independent experiments.
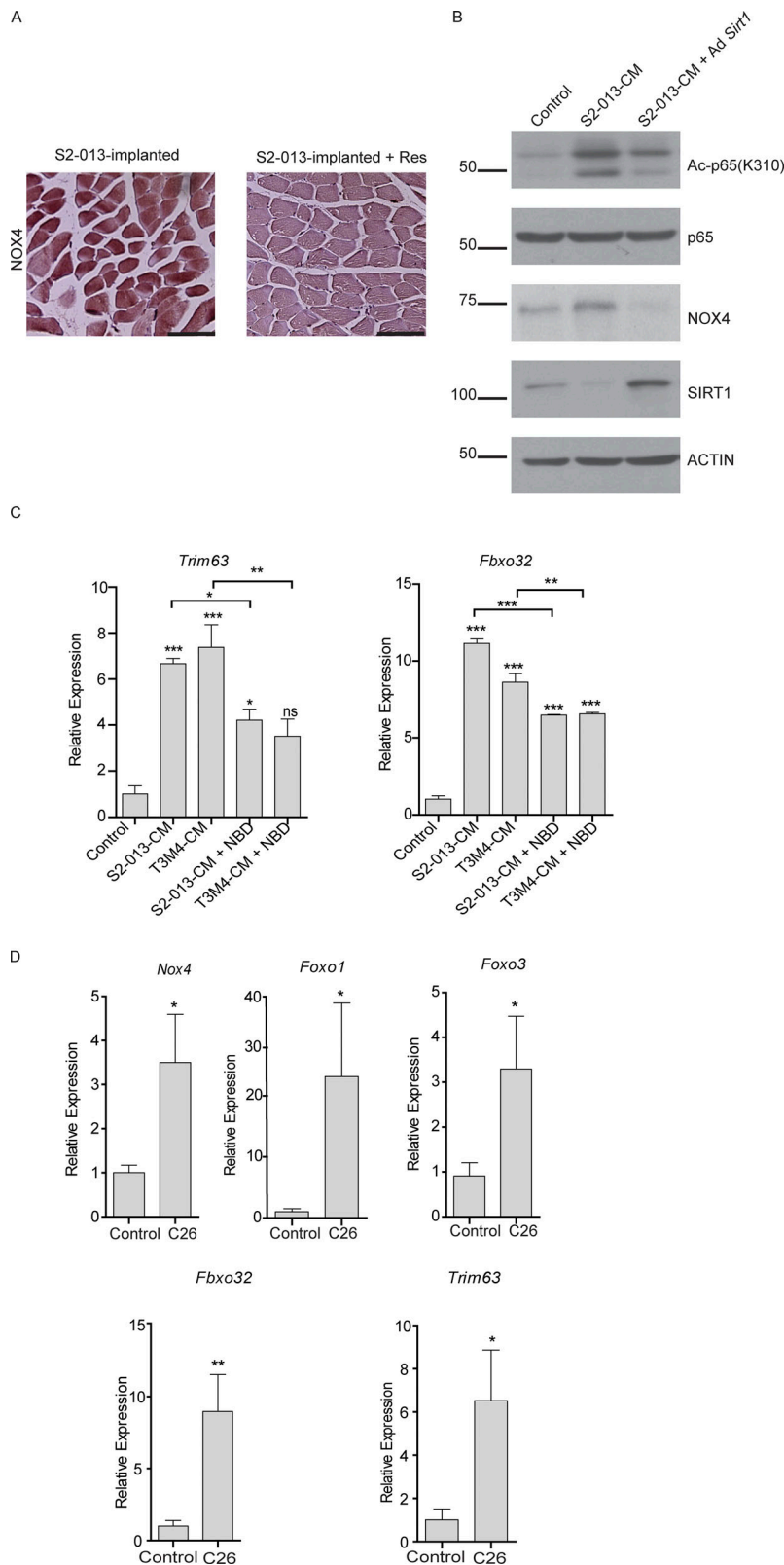
Figure S4. **Evaluation of NOX4 and atrophy markers upon SIRT1 stabilization and NF-κB inhibition. (A)** Representative images of NOX4-stained sections of gastrocnemius muscles of S2-013-implanted mice with and without resveratrol treatment. Scale bars represent 116.9 µm. **(B)** Immunoblots of C2C12 myotubes treated with S2-013 CM with and without Sirt1 overexpression. **(C)** mRNA levels of *Trim63* and *Fbxo32* in C2C12 myotubes treated with cancer cell CM and NBD for 24 h. **(D)** mRNA levels of *Nox4, Foxo1, Foxo3, Fbxo32, and Trim63* in the gastrocnemius muscles of healthy control and C26 tumor-bearing mice (*n* = 5 in each group). Data are mean ± SEM compared with one-way ANOVA with Bonferroni's (C) multiple comparisons or Student's *t* test (D). *, P < 0.05; **, P < 0.01; ***, P < 0.001. In vitro experiments were verified in at least two independent experiments.

Dasgupta et al.
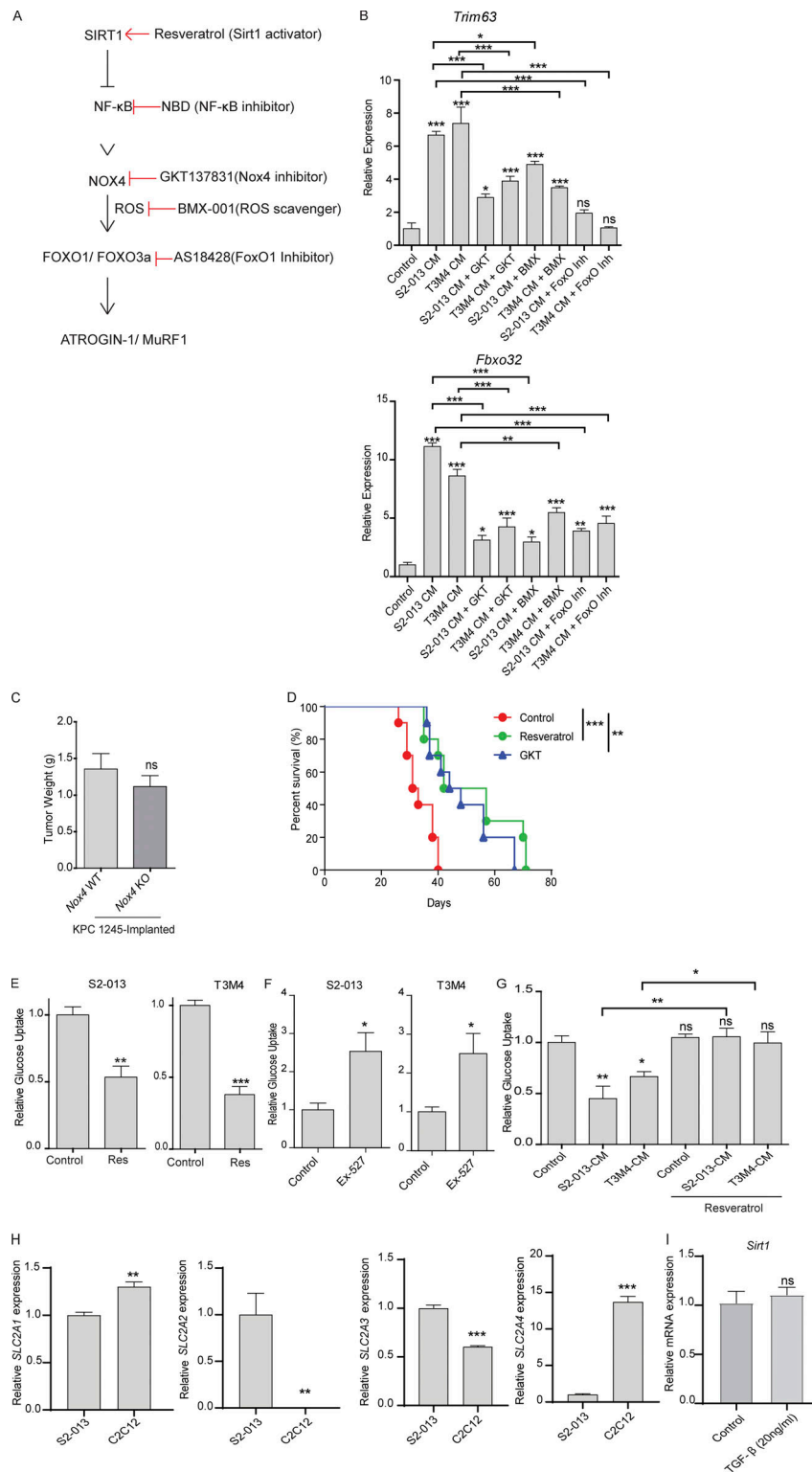Targeting Sirt1–Nox4 signaling in cancer cachexia

Journal of Experimental Medicine S5
https://doi.org/10.1084/jem.20190745

Figure S5. **The SIRT1–NOX4 axis of myodegeneration**. **(A)** Schematic illustration of the proposed pathway. **(B)** mRNA levels of *Trim63* and *Fbxo32* in C2C12 myotubes treated with control or cancer cell CM with solvent control or GKT137831 (10 μM), AS1842856 (0.1 μM; FOXO1 inhibitor), and BMX-001 (1 μM) for 24 h. **(C)** Postnecropsy tumor weights from tumor-implanted *Nox4* WT and *Nox4* KO mice. **(D)** Kaplan-Meier survival analysis of S2-013 tumor-bearing mice treated solvent control, GKT137831 (GKT), or resveratrol (*n* = 10 mice in each group). **(E)** Relative glucose uptake in S2-013 and T3M4 cells upon resveratrol treatment (50 μM) for 24 h. **(F)** Glucose uptake in S2-013 and T3M4 cells upon Ex-527 (0.5 μM) treatment for 24 h. **(G)** Glucose uptake in C2C12 myotubes upon treatment with cancer cell CM with solvent control or resveratrol for 24 h. **(H)** mRNA expression of *SLC2A1-4* in S2-013 cells and C2C12 myotubes. **(I)** mRNA expression of *Sirt1* in the C2C12 myotubes upon treatment with solvent control or TGF-β (20 ng/ml) for 24 h. Data are mean ± SEM compared with one-way ANOVA with Bonferroni's (B and G) multiple comparisons, Student's *t* test (C, E, F, H, and I), or log-rank (Mantel-Cox) test (D). *, P < 0.05; **, P < 0.01; ***, P < 0.001. In vitro experiments were verified in at least two independent experiments.

Tables S1 and S2 are provided online as separate Word documents. Table S1 lists patient characteristics. Table S2 lists primer sequences used.